Reprinted from

REVIEW OF SCIENTIFIC INSTRUMENTS

Vol. 68, No. 12, December 1997

Fiber Bragg gratings

Andreas Othonos
Department of Natural Sciences; Physics, University of Cyprus, Nicosia, Cyprus

pp. 4309-4341

AMERICAN INSTITUTE OF PHYSICS

Fiber Bragg gratings

Andreas Othonos[a)]
Department of Natural Sciences; Physics, University of Cyprus, Nicosia, Cyprus

(Received 10 March 1997; accepted for publication 12 September 1997)

Since the discovery of photosensitivity in optical fibers there has been great interest in the fabrication of Bragg gratings within the core of a fiber. The ability to inscribe intracore Bragg gratings in these photosensitive fibers has revolutionized the field of telecommunications and optical fiber based sensor technology. Over the last few years, the number of researchers investigating fundamental, as well as application aspects of these gratings has increased dramatically. This article reviews the technology of Bragg gratings in optical fibers. It introduces the phenomenon of photosensitivity in optical fibers, examines the properties of Bragg gratings, and presents some of the important developments in devices and applications. The most common fabrication techniques (interferometric, phase mask, and point by point) are examined in detail with reference to the advantages and the disadvantages in utilizing them for inscribing Bragg gratings. Reflectivity, bandwidth, temperature, and strain sensitivity of the Bragg reflectors are examined and novel and special Bragg grating structures such as chirped gratings, blazed gratings, phase-shifted gratings, and superimposed multiple gratings are discussed. A formalism for calculating the spectral response of Bragg grating structures is described. Finally, devices and applications for telecommunication and fiber-optic sensors are described, and the impact of this technology on the future of the above areas is discussed. [S0034-6748(97)01312-9]

I. INTRODUCTION

The discovery of fiber optics has revolutionized the field of telecommunications making possible high-quality, high-capacity, long-distance telephone links. Over the past three decades, the advancements in optical fiber has undoubtedly improved and reshaped fiber-optic technology. Today, optical fibers are synonymous with the word ''telecommunication.'' In addition to applications in telecommunications, optical fibers are also utilized in the rapidly growing fields of fiber sensors, fiber lasers, and fiber amplifiers. Despite the improvements in optical fiber manufacturing and advancements in the field in general, basic optical components such as mirrors, wavelength filters, and partial reflectors have been a challenge to integrate with fiber optics. Recently, however, all these have changed with the ability to alter the core index of refraction in a single-mode optical fiber by optical absorption of UV light. This photosensitivity of optical fibers allows the fabrication of phase structures in the core of fibers. These phase structures, or phase gratings are obtained by permanently changing the index of refraction in a periodic pattern along the core of the fiber. A periodic modulation of the index of refraction in the fiber core acts like a selective mirror for the wavelength that satisfies the Bragg condition. In other words, it forms a fiber Bragg grating. The grating period and length, together with the strength of the modulation of the refractive index, determine whether the grating has a high or low reflectivity over a wide or narrow range of wavelengths. Therefore, these parameters determine whether the Bragg grating acts as a wavelength division multiplexer in telecommunications, a narrow-band high-reflectance mirror in laser or sensor applications, or a wavelength-selective filter removing unwanted laser frequencies in fiber amplifiers.

The first observations of index of refraction changes were noticed in germanosilica fibers and were reported by Hill and co-workers[1,2] in 1978. They described a permanent grating written in the core of the fibers by the argon ion laser line at 488 nm launched into the fiber. This particular grating had a very weak index modulation, which was estimated to be of the order of 10^{-6} resulting in a narrow-band reflection filter at the writing wavelength.

Photosensitivity in optical fibers remained dormant for several years after its discovery by Hill *et al.*[1] mainly due to limitations of the writing technique. However, a renewed interest has risen with the demonstration of the side writing technique by Meltz *et al.*[3] almost ten years later. In the last few years, groups worldwide achieved breakthroughs in direct optical inscription of high-quality gratings into the core of optical fibers using various techniques such as the interferometric, phase mask, and point-by-point exposure to ultraviolet laser light. Gratings with a wide range of bandwidths and reflectivities can be formed on time scales ranging from a few nanoseconds (duration of the laser pulse) to a few minutes, depending on the characteristics required. These gratings are low-loss in-line fiber devices that can be written into the core noninvasively when and where desired, offering narrow-band wavelength selection to precise specifications.

Fiber-optic photosensitivity has, indeed, opened a new

a)Electronic mail: othonos@ucy.ac.cy

era in the field of fiber-optic based devices.[4–6] Innovating new Bragg grating structures find their way in telecommunication and sensor applications. Devices like fiber *Fabry–Perot Bragg gratings* for bandpass filters, *chirped gratings* for dispersion compensation and pulse shaping in ultrashort work, and *blazed gratings* for mode converters are becoming routine applications. Fiber-optics sensing is an area that has embraced Bragg gratings since the early days of its discovery. Fiber Bragg gratings have become almost synonymous with the field itself. Most fiber-optics sensor systems today make use of Bragg grating technology.

With in a few years from the initial development, fiber Bragg gratings have moved from laboratory interest and curiosity to the brink of implementation in optical communication and sensor systems. In a few years, it may be as difficult to think of fiber-optic systems without fiber Bragg gratings as it is to think of bulk optics without the familiar laboratory mirror.

This review article covers the technology of Bragg gratings in optical fibers. It introduces the phenomenon of photosensitivity in fibers, examines the properties of Bragg gratings, fabrication techniques, and presents some of the important developments in devices and applications. Section II gives a brief overview of photosensitivity in optical fibers. It covers areas such as defects in optical fibers, enhancement techniques in photosensitivity, and the major accepted mechanisms of photosensitivity. In Sec. III, a description of the most popular and efficient techniques for inscribing Bragg gratings in optical fibers is given. Techniques such as interferometric, phase mask, and point by point are described in detail. Section IV describes the various properties of Bragg gratings and different types of grating structures, some of which are blazed gratings, chirped gratings, and type II Bragg gratings. In Sec. V, a description of the *T* matrix formalism for simulating the spectral response of Bragg gratings is given. Using this formalism, a few simulations of some common Bragg grating structures with various parameters are calculated. Finally, Sec. VI gives a brief description of the various applications and devices using Bragg gratings in the fields of telecommunication and fiber sensors.

II. PHOTOSENSITIVITY OF FIBERS

A. History of photosensitivity and fiber Bragg gratings

Hill and co-workers[1,2] discovered photosensitivity in germanium-doped silica fiber at the Communication Research Center in Canada. During an experiment that was carried out to study the nonlinear effects in a specially designed optical fiber, visible light from an argon ion laser was launched into the core of the fiber. Under prolonged exposure, an increase in the attenuation of the fiber was observed. Following that observation, it was determined that the intensity of the light back reflected from the fiber increased significantly with time during the exposure. This increase in reflectivity was the result of a permanent refractive-index grating being photoinduced in the fiber. This new nonlinear photorefractive effect in optical fibers was called fiber photosensitivity. In their experiment,[1] the 488 nm laser light that

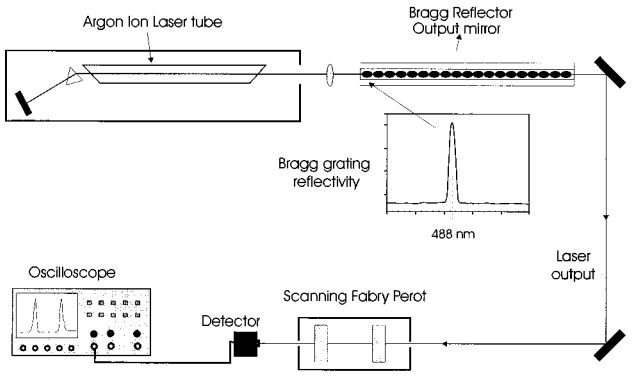

FIG. 1. Distributed feedback cw argon ion laser. The fiber reflection filter (its reflection spectral response is shown) takes the place of the output reflector giving rise to narrow-band oscillation (after Ref. 1).

was launched into the core of a specially designed fiber interfered with the Fresnel reflected beam (4% reflection from the cleaved end of the fiber) and initially formed a weak standing-wave intensity pattern. The high intensity points altered the index of refraction in the photosensitive fiber core permanently. Thus, a refractive-index perturbation that had the same spatial periodicity as the interference pattern was formed, with a length only limited by the coherence length of the writing radiation. This refractive-index grating acted as a distributed reflector that coupled the forward propagating to the counterpropagating light beams. The coupling of the beams provided positive feedback, which enhanced the strength of the back-reflected light, and thereby increased the intensity of the interference pattern, which in turn increased the index of refraction at the high intensity points. This process was continued until eventually the reflectivity of the grating reached a saturation level. These gratings were, thus, called *self-organized* or *self-induced* gratings since they formed spontaneously without human intervention. The specially designed fibers were supplied by Bell Northern Research, and had a small core diameter that was heavily doped with germanium.

For almost a decade after its discovery, research on fiber photosensitivity was pursued sporadically only in Canada using the special Bell Northern research fiber. During this time, Lam and Garside[7] (1981) showed that the magnitude of the photoinduced refractive index change depended on the square of the writing power at the argon ion wavelength (488 nm). This suggested a two-photon process as the possible mechanism of refractive-index change. The lack of international interest in fiber photosensitivity at the time was attributed to the effect being viewed as a phenomenon present only in this special fiber. Almost a decade later, Stone[8] proved otherwise; he observed photosensitivity in many different fibers, all of which contained a relatively high concentration of germanium.

Self-organized Bragg gratings are in effect narrow-band reflection filters in optical fibers. Hill and co-workers[1] used one of these gratings in place of the output reflector of an argon ion laser and were able to obtain stable cw oscillation at 488 nm (see Fig. 1). This represented the first reported demonstration of distributed feedback oscillation of a gas laser operated in the visible region of the spectrum. The out-

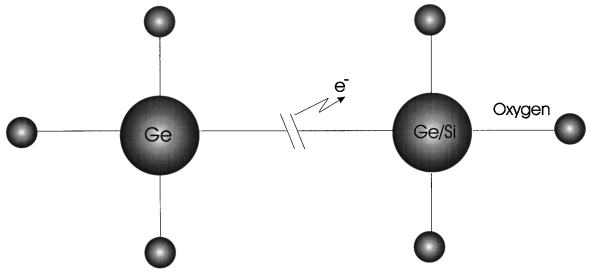

FIG. 2. Oxygen-deficient germania defects thought to be responsible for the photosensitive effect in germania-doped silica. An electron is released on breaking of the bond.

put reflector was removed from the laser head and a microscope objective lens was used to couple the beam into the core of the optical fiber containing the reflection filter.

Although the discovery of photosensitivity in the form of photoinduced index changes played a key role in the advancements of optical fiber technology, devices such as the *self-induced* gratings were not practical. This was because the Bragg resonance wavelength was limited to the argon ion wavelength (488 nm). Slight tunability in the resonance wavelength could be achieved by longitudinally straining the fiber during the Bragg grating formation process. However, this method does not allow the fabrication of gratings that have resonance wavelengths in the infrared region, which is of interest in optical communications. Moreover, in the blue-green wavelength regions, these gratings are intrinsically unstable owing to the continuing photosensitivity of the fiber. This causes the grating to continually evolve during its use as a Bragg reflector. The grating can even disappear completely if it is exposed to light of a different blue-green wavelength.[9] A further problem with self-induced gratings is their small photoinduced refractive-index change (due to the two-photon process). Therefore, to achieve detectable reflectivities, long gratings are required, thus, making these types of gratings not useful for localized sensing.

In 1989, Meltz *et al.*[3] showed that a strong index of refraction change occurred when a germanium-doped fiber was exposed to UV light close to the absorption peak of a germania-related defect at a wavelength range of 240–250 nm. Figure 2 shows an oxygen-deficient germania defect thought to be responsible for the photosensitivity in germania-doped silica. The peak wavelength of absorption of the well-known GeO defect is at $\sim$240 nm.[10] This absorption has been shown to bleach when exposed to UV radiation,[11,12] as shown in Fig. 3. Hand and Russel[13] developed a model to explain the change in the index of refraction by relating it to the absorption changes via the Kramer–Kronig relationship. The model proposed the breaking of the GeO defect resulting in a GeE′ center with the release of an electron, which is free to move within the glass matrix until it is retrapped.

Fibers, other than the ones doped with germanium, also exhibit photosensitivity phenomena. Fibers doped with europium,[14] cerium,[15] and erbium:germanium (Ref. 16) show varying degrees of sensitivity in a silica host optical fiber, but none is as sensitive as the germania. One fiber doping producing large index modulations (of the order of 10^{-3}) is

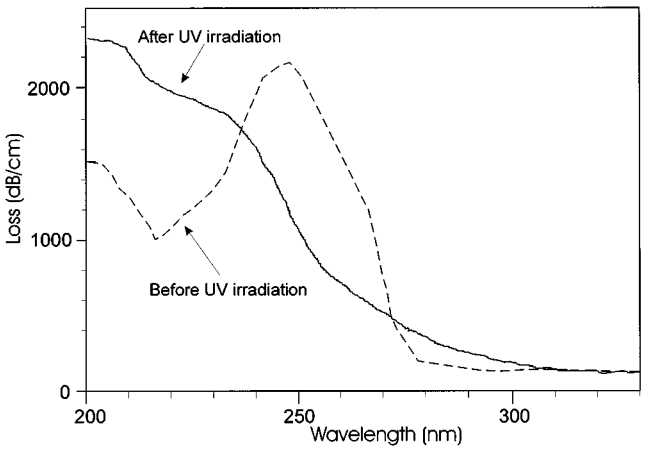

FIG. 3. Transmission loss spectrum of a 15 μm thick preform before and after being irradiated by 244 nm UV radiation (after Ref. 11).

germanium–boron codoping.[17] Photosensitivity has also been observed in a fluorozirconate fiber[18] doped with cerium:erbium, where Bragg gratings were inscribed using 246 nm radiation.

B. Defects in germanosilica optical fibers

The fact that the change of the index of refraction in a germanosilica fiber is triggered by a single photon at $\sim$240 nm, which is well below the band gap at 146 nm, implies that the point defects in the ideal glass tetrahedral network are responsible for this process.

Defects in optical fibers first attracted attention because of the unwanted absorption band associated with them, which caused transmission losses. These defects are often called color centers due to their strong absorption. Normally, these defects are caused by the fiber drawing process,[19] and ionizing radiation.[20] A great deal of research[21] has been directed in minimizing the formation of these defects. However, with their implication to fiber Bragg gratings, the role of the defects in optical fibers has changed dramatically.

Experimental results suggest that Ge–Si *wrong bonds* are responsible for the photosensitivy of modified chemical vapor deposition (MCVD) germanosilica fiber. Although it appears that the Ge–Si wrong bond has a high efficiency for triggering the processes responsible for the index change in the glass, it must be made clear that Ge–Si bonds may not be the only trigger mechanism, just the most efficient found so far. The Ge–Si *wrong bond* has an absorption band at $\sim$240 nm.[22] Ultraviolet light processing leads to a bleaching of this absorption band,[23] resulting in the creation of new defects, and hence, the evolution of new absorption bands. The creation of defect bands has been reported[22,24,25] centered at 195, 213, and 281 nm. The radiation induced defect centers were identified and characterized by electron spin resonance spectroscopy (ESR). In 1986, Friebele and Griscom[25] were the first to report on what is now termed the $Ge(1)^-$, $Ge(2)^-$, and GeE′ defect centers. The $Ge(1)^-$ and $Ge(2)^-$ centers are composed of an electron trapped at a four coordinated Ge substitutional for Si in the SiO_2 tetrahe-

dral network, with the $Ge(1)^-$ center being coordinated to four O–Si bonds, and the $Ge(2)^-$ center to one O–Ge and three O–Si bonds.[26] The GeE′ center is axially symmetric, consisting of an unpaired electron trapped at an oxygen vacancy in the sp^3 orbital of a single germanium back bonded to three neighboring oxygens forming a trigonal pyramid.

It is well established that the Ge–Si and Ge–Ge *wrong bonds* are responsible for the photosensitivity of germanosilica glass. Photoionization of the *wrong bonds* triggers the processes responsible for the index change in fiber. Irradiation with ~240 nm UV light ionizes a *wrong bond* to form a GeE′ center. The electron released in this process may recombine immediately with its GeE′ center to give recombination luminescence, or it may diffuse through the matrix until it becomes trapped at a Ge(1) of Ge(2) center to form a $Ge(1)^-$ or $Ge(2)^-$ center, respectively.[27,28]

C. Enhanced photosensitivity in silica optical fibers

Photosensitivity of optical fibers may be thought of as a measure of the amount of change that can be induced in the index of refraction in a fiber core following a specific exposure of UV light. Since the discovery of photosensitivity and the first demonstration of grating formation in germanosilica fibers, there has been considerable effort in understanding and increasing the photosensitivity in optical fibers. Initially, optical fibers that were fabricated with high germanium dopant levels or under reduced oxidizing conditions were proven to be highly photosensitive. Recently, *hydrogen loading (hydrogenation)*, *flame brushing*, and *boron codoping* have been used for enhancing the photosensitivity of germanosilica fibers. In addition to the above techniques, exposure with 193 nm ArF excimer laser radiation proved to be an alternative method for inscribing strong Bragg gratings in fibers without the need of H_2 loading. This method may be thought as a photosensitive enhancement technique to the usual 240–250 nm band irradiation for inscribing Bragg gratings in germanosilica fibers.

1. Hydrogen loading/hydrogenation

Hydrogenation or hydrogen loading of optical fibers is a simple technique for achieving very high UV photosensitivity in germanosilica optical fibers. Hydrogen loading[29] is carried out by diffusing hydrogen molecules into fiber cores at high pressures and temperatures. This technique, which enhances photosensitivity, allows permanent changes in the fiber core index of refraction (as high as 0.01) following UV irradiation (this change is of the same order as the core/cladding index difference). It should be noted that the increased fiber/waveguide photosensitivity as a result of hydrogen loading is not a permanent effect, and as the hydrogen diffuses out, the photosensitivity decreases.

Measurements of spectral response in the infrared of UV irradiated hydrogenated samples indicated the formation of OH absorbing species. On the other hand, UV irradiation of untreated samples showed no OH formation.[29,30] It appears the hydrogen molecules react in the glass at normal Si–O–Ge sites, forming OH species and UV bleachable germanium oxygen deficiency centers, which are responsible for the enhanced photosensitivity. Optical absorption spectra of a germanosilica preform rod heated in a hydrogen atmosphere at 500 °C for different times are shown in Fig. 4.[31] The growth of the broad 240 nm absorption band is clearly evident. This indicated that the reaction of hydrogen molecules at Ge sites produced germanium–oxygen deficiency centers assigned to the broad 240 nm absorption band.

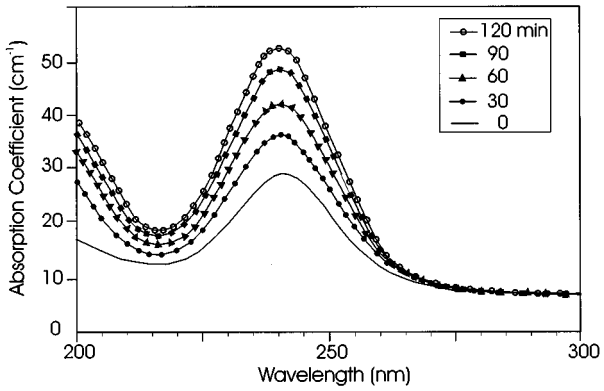

FIG. 4. Optical absorption spectra of a germanosilica preform rod heated in a H_2 atmosphere at 500 °C for different times (after Ref. 31).

Figure 5 shows the absorption spectrum changes in the infrared for a germanosilica fiber exposed to 1 atm pressure of hydrogen gas at 100 °C. The sharp absorption peak at 1.24 μm, due to molecular hydrogen, is saturated after 10 h. The absorption band due to OH formation, is comprised of two absorption peaks[32] closed together, which emerge in the spectra after 10 h of treatments [absorption peaks at 1.39 μm (Si–OH) and 1.41 μm (Ge–OH)]. This indicates that hydrogen molecules react with germanosilica glass and form OH absorbing species. Figures 4 and 5 suggest that the germanium–oxygen deficiency centers and OH species are formed from thermally driven reactions between hydrogen and germanosilica glass. The inscription of Bragg gratings in hydrogen loaded fiber undoubtedly involves both thermal and photolytic mechanisms. Atkins and his co-workers[30] investigated the thermal effects by exposing germanosilica glass (loaded 1 mol % hydrogen) to a CO_2 laser operating in a cw mode for 10 s. The CO_2 laser beam was absorbed by

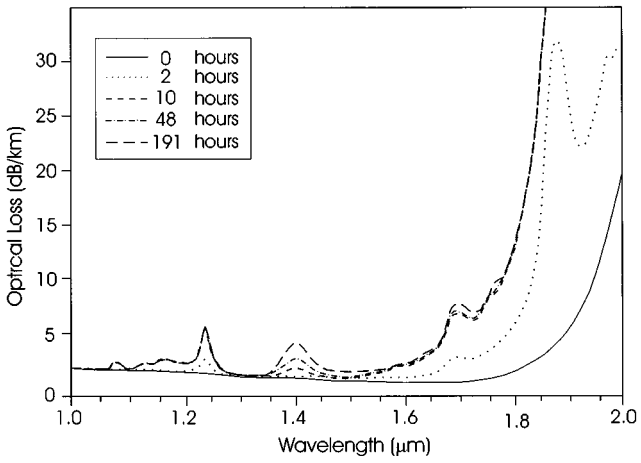

FIG. 5. Absorption spectrum changes in the IR for a germanosilicate fiber exposed to 1 atmospheric pressure of hydrogen gas at 100 °C (after Ref. 31).

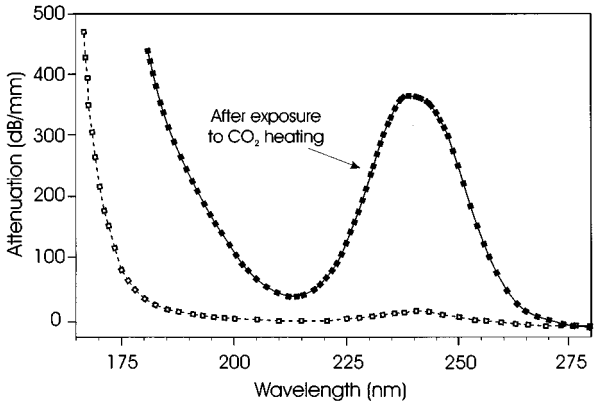

FIG. 6. UV spectra of 1 mol % H_2 loaded germanosilicate glass before (□) and after (■) 10 s exposure to a CO_2 laser beam (after Ref. 30).

the glass, resulting in equivalent heat of 600 °C. The UV absorption spectrum, shown in Fig. 6, clearly shows growth of the germanium–oxygen deficiency-center band near 240 nm, from 20 dB/mm before heating to 380 dB/mm after heating.

The simplest mechanism envisioned for the formation of Bragg gratings in hydrogen-loaded germanosilica fibers during UV irradiation is that of primary thermally driven reactions forming germanium–oxygen deficiency centers. This is followed by an immediate UV bleaching of the germanium–oxygen deficiency centers giving rise to index changes. There are several advantages of enhancing fiber photosensitivity through ''hydrogen loading.'' The first and foremost advantage is that hydrogenation allows strong Bragg gratings to be fabricated in any germanosilica fiber, including standard telecommunications fibers that typically have low germanium concentration, and hence, low intrinsic photosensitivity. Second, permanent changes occur only in regions that are UV irradiated. Finally, unreacted hydrogen in other sections of the fiber slowly diffuses out. Thus, leaving negligible absorption losses at the optical communication windows.

It should be pointed out that the tail of the OH broadband absorption peak at 1.39 and 1.41 μm resulting from gratings written in H_2 loaded standard single-mode optical fibers introduces losses, which are often unacceptable to telecommunication network systems designers. However, by loading fiber with deuterium instead of hydrogen, the UV induced absorption peak is shifted to longer wavelengths, out of the erbium amplifier band of 1.55 μm.[33]

2. Flame brushing

Flame brushing is a simple technique for enhancing the photosensitivity in germanosilica fiber.[34] The region of the optical waveguide to be photosensitized is brushed repeatedly by a flame fueled with hydrogen (hydrogen-rich flame) and a small amount of oxygen. The flame reaches a temperature of approximately 1700 °C. The photosensitization process takes approximately 20 min to complete. At these temperatures, the hydrogen diffuses into the core of the fiber very quickly and reacts with the germanosilica glass to produce germanium–oxygen deficiency centers. This creates a strong absorption band at 240 nm in the Ge-doped core, rendering the core highly photosensitive so that UV light can induce a significant change in its refractive index. This flame-brush technique has been used to increase the photosensitivity of standard telecommunications fiber by a factor greater than 10, achieving[34] changes in the index of refraction $>10^{-3}$. The enhanced photosensitivity techniques of flame brushing and hydrogen loading follow the same concept. In both cases, hydrogen is used in a chemical reaction with germanosilica glass to form germanium–oxygen deficiency centers that are responsible for the photosensitivity. The formation of Bragg gratings in flame-brushed germanosilica fibers undoubtedly involves both thermal and photolytic mechanisms, except in this case, the thermally driven chemical reactions occur simultaneously as the hydrogen diffuses into the core at elevated temperatures. Subsequent UV irradiation then bleaches the germanium–oxygen deficiency center band giving rise to index changes.

There are several advantages in enhancing fiber photosensitivity by the flame-brushing technique. The increased photosensitivity in the fiber is permanent, as opposed to hydrogen loading where the fiber loses its photosensitivity as the hydrogen diffuses out of the fiber. It allows strong Bragg gratings to be fabricated in standard telecommunications fibers that typically exhibit no intrinsic photosensitivity. Localization of photosensitivity due to the relatively small flame can be used to brush the fiber. However, one major drawback in this technique is that the high-temperature flame weakens the fiber.

3. Boron codoping

Boron as a codopant in germanosilica fiber enhances UV photosensitivity in optical fibers.[35] A comparison of the relative photosensitivity of four different types of fibers including boron codoping is given in Table I. The fibers were irradiated with modest power intensities of 1 W/cm^2 from a frequency-doubled cw argon ion laser until the grating reflectivity saturated. The results showed that the fiber containing boron had an enhanced photosensitivity. This fiber was much more photosensitive than the fiber with higher germanium concentration and without boron. In addition, saturated index changes were higher and achieved faster than for any of the other fibers. This implies that there is an additional mechanism operating in the boron-codoped fiber, which enhances the photoinduced refractive-index changes.

The germanium–boron-codoped fiber (Table I) was fabricated with a germanium composition of 15 mol %. In the absence of boron, this fiber would have a refractive-index difference of 0.025 between the core and cladding. However, when the preform was drawn into fiber, the measure value for Δn dropped to 0.003. It appears that the addition of boron reduces the core index of refraction. This result is not surprising, as it is known that the addition of boron oxide to silica can result in a compound glass that has a lower index of refraction than that of silica.[36] Studies have shown that the boron-doped silica glass system results in lower refractive-index values when the glass is quenched, while subsequent thermal annealing causes the refractive index to increase.

TABLE I. Photosensitivity comparison of four different types of fiber (Ref. 35).

Fiber design	Fiber Δn	Saturated index modulation	Maximum reflectivity for 2 mm Bragg grating	Time for reflectivity to reach saturation
Standard low-loss fiber 4 mol % germania	0.005	3.5×10^{-5}	1.2%	2 h
High index fiber 20 mol % germania	0.03	2.5×10^{-4}	45%	2 h
Reduced fiber 10 mol % germania	0.01	5×10^{-4}	78%	1 h
Boron-codoped fiber 15 mol % germania	0.003	7×10^{-4}	95%	10 min

This is consistent with the fact that Δn dropped from 0.025 to 0.003 when the preform was drawn into fiber, since fibers are naturally quenched during the drawing process. This effect is assumed to be due to a buildup in thermoelastic stresses in the core of the fiber, resulting from the large difference in thermomechanical properties between the boron-containing core and the silica cladding. It is well known that tension reduces the refractive index through the stress-optic effect. Ultraviolet absorption measurements of the fiber between 200 and 300 nm showed only the characteristic germanium–oxygen deficiency-center peak at 240 nm. The boron codoping did not affect the peak absorption at 240 nm, nor the shape of the 240 nm peak, and no other absorption peaks were observed in this wavelength range.[35] The absorption measurements suggest that boron codoping does not enhance the fiber photosensitivity through production of germanium–oxygen deficiency centers as in the case of hydrogen loading and flame-brushing techniques. Instead, it is believed that boron codoping increases the photosensitivity of the fiber by allowing photoinduced stress relaxation to occur. In view of the stress induced refractive-index changes known to occur in boron-doped silica fibers, it seems likely that the refractive index increases through photoinduced stress relaxation initiated by the breaking of the wrong bonds by UV light.

Table II shows a comparison of photosensitivity of various fibers and enhancing techniques.[37] The results show that standard telecommunication fibers are not very photosensitive, showing little difference between different varieties of standard fiber. The higher germanium-doped Corning ''*payout*'' fiber is more photosensitive than standard fibers, but is much less effective than a standard fiber that has enhanced photosensitivity.

4. ArF excimer vacuum UV radiation

Photosensitivity, and hence, the inscription of Bragg gratings in optical fibers has been associated with the bleaching of an absorption band located near 5.0 eV (245 nm band). Recently, however, it has been demonstrated that Bragg grating devices can be inscribed in telecommunication fibers using the ArF excimer vacuum UV radiation at 193 nm.[38,39] Albert and co-workers[38] fabricated fiber Bragg gratings using a KrF (248 nm) and ArF (193 nm) excimer laser light with a phase mask. Bragg gratings fabricated using 193 nm irradiation appeared to develop much stronger reflectivity than gratings inscribed with 248 nm under similar excitation conditions. It is clear from their results that the 193 nm excimer laser source provides an efficient technique for inscribing refractive-index patterns in Ge-doped silica fibers. An advantage of using shorter-wavelength light in inscribing Bragg gratings is the possibility of higher spatial resolution in diffraction-limited techniques, such as the point-by-point writing.

D. Mechanism of photoinduced refractive index change

Bragg gratings have been written in many types of optical fibers using various methods, however, the mechanism of index change is not fully understood. Several models have been proposed for these photoinduced refractive-index changes. The only common elements in these theories is that

TABLE II. Comparison of the photosensitivity of various fibers and enhancing techniques (Ref. 37).

Fiber type	GeO_2 in fiber core mol %	Reflectivity of 1.5 mm Bragg grating %	Time required to inscribe the grating
Philips, matched cladding	5	17	60 min
Philips, depressed cladding	4	20	60 min
Deeside fiber	5	17	60 min
Corning payout fiber	8	29	90 min
Hydrogenated standard fiber	4	60	10 min
High index fiber	20	77	10 min
Reduced fiber	12	97	5 min
Boron codoped	17	91	1 min
Hydrogenated boron-codoped fiber	17	87	10 s

the germanium–oxygen vacancy defects, Ge–Si or Ge–Ge (the so-called ''*wrong bonds*'') are responsible for the photoinduced index changes.

During the high-temperature gas-phase oxidation process of the modified chemical vapor deposition technique, GeO_2 dissociates to GeO due to its higher stability at elevated temperatures. This species, when incorporated into the glass, can manifest itself in the form of oxygen vacancy Ge–Si and Ge–Ge ''wrong bonds.'' Since highly doped germanosilica core optical fibers are photosensitive to UV radiation in the range of 240–250 nm, these oxygen vacancy defects have been directly linked to the mechanism of photoinduced refractive-index changes in each of the proposed models. Although there is experimental evidence for the validity of some of the proposed models, there are conflicting reports regarding their calculated contribution to the measured induced refractive-index change. It is believed that more than one process is involved in the photoinduced refractive-index changes, and hence, to the grating formation dynamics. Below, some of the proposed models will be discussed.

1. Color center model

The color center model assumes that photoinduced changes in the absorption spectrum give rise to change in the index of refraction through the Kramers–Kronig relationship. The Kramers–Kronig relationship given as[28]

$$\epsilon_r(\lambda)=1+\int \frac{\epsilon_i(\lambda)}{\lambda'-\lambda}\,d\lambda', \tag{2.1}$$

relates the real and imaginary parts of the dielectric constant $\epsilon=\epsilon_\rho+\imath\epsilon_1=(n+\imath\kappa)^2$, where n is the refractive index and κ is the absorption index. The relationship arises from the causality condition for the dielectric response and demonstrates that the index change produced in the infrared/visible region of the spectrum by the photoinduced processing results from a change in the absorption spectrum of the glass in the UV/far-UV spectral region.

In this model, proposed by Hand and Russell,[13] UV exposure changes the material properties of the glass and introduces new electronic transitions of defects (color centers). The underlying premise of this model is that the photosensitive effect arises from localized electronic excitations of defects. The wrong-bond defects, which initially absorb the light, are transformed to defects that are more polarizable by virtue of the fact that their electronic transitions occur at longer wavelengths or have stronger transitions.

According to the color center model, the refractive index at a point is related only to the number density and orientation of defects in that region and is determined by their electronic absorption spectra.

Williams and co-workers[11] measured the changes, between 200 and 350 nm, in the absorption spectrum of germanosilica glass fibers that were irradiated with UV light. The inferred refractive-index change using the Kramers–Kronig calculation was within a factor of 3 of that estimated from the reflectivity of the Bragg grating. Atkins and Mizrahi[12] reported on the absorption spectrum, between 200 and 300 nm, of a fiber core before and after inscribing a

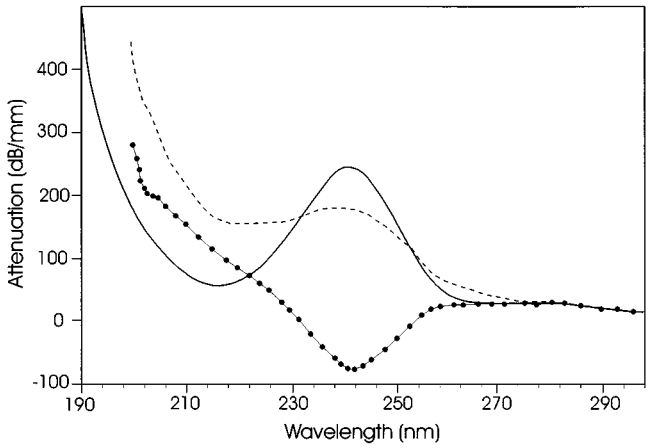

FIG. 7. UV absorption spectra before (solid line) and after (dashed line) writing an 81% peak reflectivity grating in an AT&T Accutether single-mode fiber. The change in attenuation (solid circles) is also shown (after Ref. 12).

Bragg grating with 81% reflectivity (see Fig. 7). The band at 241 nm is partially bleached and new absorption bands arise. Using the Kramers–Kronig relation, the observed changes in the absorption spectrum indicated that only 16% of the index change inferred from the reflectivity of the grating can be accounted for. It seems that the attenuation at wavelengths below 200 nm, which could not be measured due to measurement limitations, could be responsible for a substantial part of the index change.

Atkins *et al.*[24] reported a more detailed study of absorption changes in optical fiber preforms cores. They measured absorption changes between 165 and 300 nm, for 3 mol % germania MCVD optical fiber preform cores before and after UV exposure. The absorption changes observed in the region of 200–300 nm, were consistent with those previously reported[12] when phase gratings were written into fibers. Figure 8 shows the UV absorption spectra of the optical fiber preform core before [Fig. 8 (i)], and after 30 min UV exposure [Fig. 8 (ii)]. The induced UV spectra changes are shown in Fig. 8 (iii). It is evident that the 240 nm band is bleached, and a strong and broad absorption band centered at ~195 nm

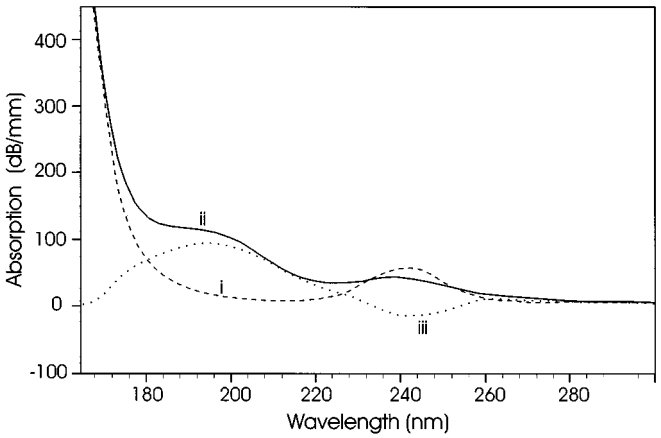

FIG. 8. UV absorption spectra of 3 mol % germania MCVD optical fiber preform core (i) before and (ii) after 30 min of UV exposure. The induced UV spectral changes are shown in (iii) (after Ref. 24).

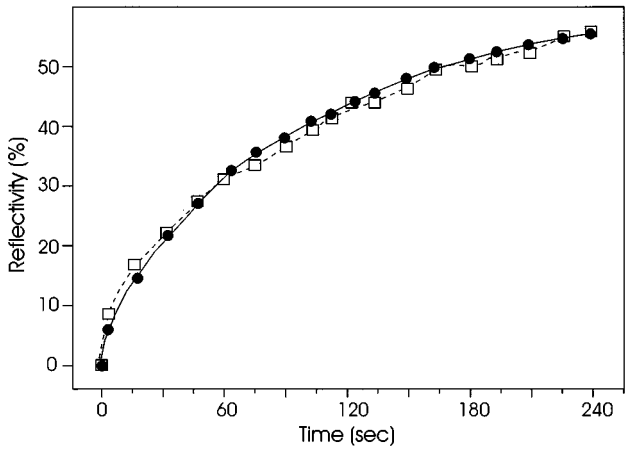

FIG. 9. Growth rate of Bragg gratings written in AT&T Accutether fiber (10 mol % germania). Initial writing (solid circles) second writing after first grating is thermally erased (squares) (after Ref. 25).

is present. It is believed that this absorption band corresponds to the GeE′ center. Kramers–Kronig calculations of the absorption changes shown in Fig. 8 resulted in a calculated index change, which was in good agreement with the index changes estimated from a Bragg grating written in fibers of similar composition and under the same UV exposure.

Atkins *et al.*[24] also found that the induced absorption changes could be completely reversed by heating the fiber at 900 °C for 60 min and subsequently duplicated by reexposure at the same intensity and duration used in the first exposure. Figure 9 shows the growth of a Bragg grating written in AT&T Accutether fiber (10 mol % germania) with UV exposure and upon thermal erasure by heating from a CO_2 laser. The grating was rewritten under the original UV exposure conditions. No significant change in the photosensitivity of the fiber was observed. The bleaching of the absorption band and subsequent creation of new absorption bands agrees with the redistribution of defects first suggested by Hand and Russell.[40] The fact that the absorption changes reverse as a grating is heated is consistent with mechanisms of grating formation in which the absorption changes play a major role. It is interesting to point out that their results are in conflict with other reported results[41] in which each cycle of writing and erasing a grating was found to reduce the fiber's photosensitivity. Nevertheless, there is strong evidence linking the mechanism of refractive-index changes, at least in part, to the color center model. To date, the color center model is the most widely accepted model for the formation mechanism of Bragg gratings, however, it is not clear whether this model alone can always account for all the observed index changes.

2. Dipole model

The dipole model is based on the formation of built-in periodic space-charge electric fields by the photoexcitation of defects. Photoionization of the germanium–oxygen deficient centers, Ge–Si or Ge–Ge, creates positively charged GeE′ hole centers and free electrons. The free electron diffuses away and gets trapped at neighboring Ge(1) and Ge(2)

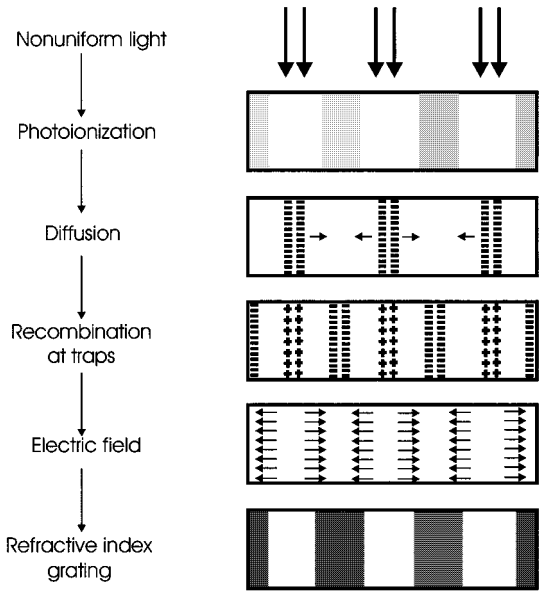

FIG. 10. Response of a photorefractive material to a sinusoidal spatial light pattern.

sites to from negatively charged $Ge(1)^-$ and $Ge(2)^-$ electron traps, respectively.[37] The GeE′ hole traps and $Ge(1)^-$ and $Ge(2)^-$ electron traps result in electric dipoles with spacing of the order of several angstroms. Each resulting dipole will produce a static dc polarization field that extends many molecular spacings. These static electric fields induce local index of refraction changes proportional to $\mathbf{E}^2$ through the dc Kerr effect. During the writing process of a Bragg grating, when the fiber is exposed to UV interference pattern, the free electrons in the high intensity regions will diffuse until they are trapped by defects in the low intensity regions. This redistribution of charges within the fiber will create periodic space-charge electric fields. The periodic refractive-index change is proportional to $\chi^{(3)}\mathbf{E}^2$, where $\chi^{(3)}$ is the third-order nonlinear coefficient, and $\mathbf{E}$ is the electric field of the dipole source. The dipole model was partly inspired by the photorefractivity models in crystals, where there is a $\pi/2$ phase shift of the index change relative to the interference pattern of the UV light as shown in Fig. 10. Although this mechanism works very well for photrefractive crystals, it might be difficult to justify in the case of photosensitive fibers due to the large number density of dipoles required (estimates of at least $4\times10^{18}\,\mathrm{cm}^{-3}$ GeE′ centers are required[42]).

3. Compaction model

The compaction model is based on laser irradiation induced density changes, which lead to index of refraction changes. Irradiation by laser light at 248 nm at intensities well below the breakdown threshold has been shown to induce thermally reversible linear compaction in amorphous silica leading to index of refraction changes. Fiori and Devine[43] used a KrF excimer laser to irradiate thin-film a-SiO_2 samples grown on Si wafers. Figure 11 shows the variation of this oxide thin-film thickness as a function of an accumulated UV dose for a nominally 100 nm oxide sample. At an accumulated dose of $2000\,\mathrm{J/cm}^2$, it is obvious that

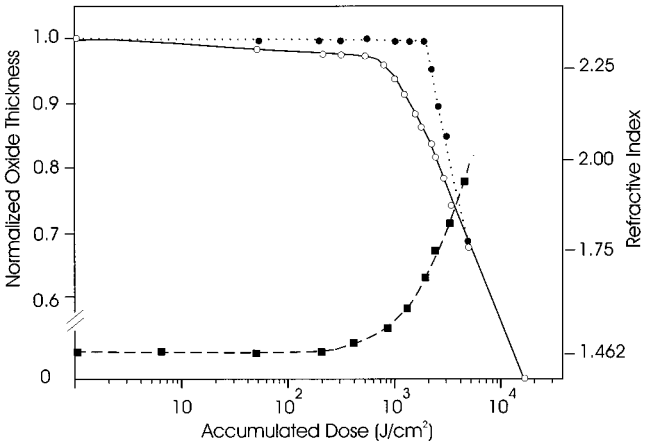

FIG. 11. Observed compaction of a 100 nm thick oxide as a function of accumulated UV dose (circle); the same sample after thermal annealing for 1 h at 950 °C in vacuum (solid circle). Evolution of the refractive index during laser irradiation (solid square) (after Ref. 43).

there is a reduction in the thickness of the film (approximately 15%) and a corresponding evolution of the refractive index during laser irradiation. After annealing for 1 h in a vacuum 10^{-6} Torr at 950 °C, the compaction disappeared and the original thickness and preirradiated refractive-index value was retrieved. Continued accumulation of UV irradiation beyond this reversible compaction regime led to irreversible compaction until the film was entirely etched after a total accumulated dose of 17 000 J/cm^2. An approximate linear relationship has been found between the index of refraction and the density change $(\Delta V/V)$ by simply transforming the measured thickness variation into a volume variation using $(\Delta V/V)=3(\Delta t/t)/(1+2\sigma)$, where σ is the Poisson's ratio and t is the thickness. Fiori and Devine[43] also measured the refractive-index variation in hydrostatically compressed silica as a function of pressure. Their results were in very good agreement with those found in laser compacted a-SiO_2, which confirmed their hypothesis that laser and hydrostatically induced compaction arise though similar physical mechanisms. This result led them to suggest that the phenomenon of compaction of a-SiO_2 proceeds through internal structural rearrangements in the material and not primarily through a process of defect creation.

The compaction model is relatively new and it has not been examined thoroughly. Although there is some work published on compaction in germanosilicate fibers, not enough is known yet in this area.

4. Stress-relief model

The stress-relief model[44] is based on the hypothesis that the refractive-index change arises from the alleviation of built-in thermoelastic stresses in the core of the fiber. The fiber-optic core in a germanosilica fiber is under tension due to the difference in the thermal expansion of the core and the cladding as the glass is cooled below the fictive temperature during fiber drawing. Through the stress-optic effect, it is known that tension reduces the refractive index and is, therefore, expected that stress relief will increase the refractive index. During UV irradiation, the wrong bonds break and promote relaxation in the tensioned glass, hence, reducing frozen-in thermal stresses in the core.

In this model, the refractive-index changes result as a consequence of stress relief in the core of the fiber. This mechanism is initiated by breakage of the ''wrong bond'' by UV light. Although there is an abundance of breakable ''wrong bonds'' in germanosilica core fibers, this is not the case for pure silica core fibers, which are not photosensitive in the UV. Like the compaction model, the stress-relief model is also relatively new and more research will be required to accurately determine its validity.

III. INSCRIBING BRAGG GRATINGS IN OPTICAL FIBERS

A. Externally written Bragg gratings in optical fibers

Inscribing Bragg gratings in optical fibers is a formidable task. The requirement of a submicron periodic pattern makes the stability a severe constraint on the techniques able to write Bragg gratings in optical fibers. To date, there are only a few externally written fabrication techniques, namely, the interferometric technique, the phase mask technique, and the point-by-point technique.

1. Interferometric fabrication technique

The interferometric fabrication technique, the first external writing technique of forming Bragg gratings in photosensitive fibers, was demonstrated by Meltz *et al.*[3] It utilized an interferometer that split the incoming UV light into two beams and then recombined them to form an interference pattern. The fringe pattern was used to expose a photosensitive fiber, inducing a refractive index modulation in the core. Bragg gratings in optical fibers have been fabricated using both amplitude splitting and wave-front-splitting interferometers. These two different types of interferometers will be examined next.

(a) *Amplitude-splitting interferometer.* In an amplitude-splitting interferometer, the UV writing laser light is split into two equal intensity beams and are later recombined after traversing through two different optical paths. This forms an interference pattern at the core of a photosensitive fiber. Cylindrical lenses are normally placed in the interferometer to focus the interfering beams to a fine line matching the fiber core. The Bragg grating period, Λ, which is identical to the period of the interference fringe pattern, depends on both the irradiation wavelength λ_w, and the half-angle between the intersecting UV beams, φ (Fig. 12).

The period of the grating is given by

$$\Lambda=\frac{\lambda_w}{2\sin\varphi}, \tag{3.1}$$

where λ_w, is the UV wavelength and φ is the half-angle between the intersection UV beams (see Fig. 12). Although the interference pattern is formed in glass (within the core of the optical fiber), its period is the same as it would be if the beams were interfering in air. This is a result of the refraction of the beams coupled with the shortening of the wavelength as they enter the glass. The Bragg condition, $\lambda_B=2n\Lambda$,

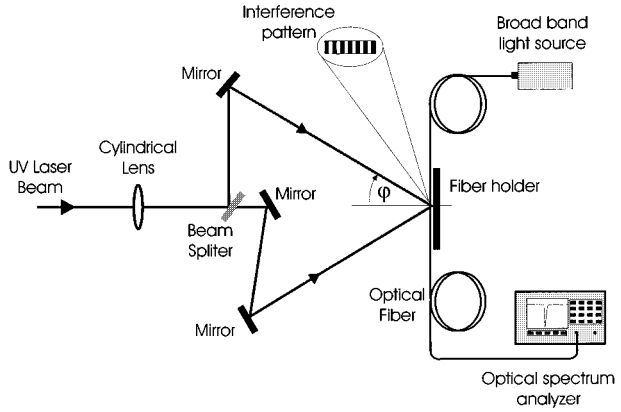

FIG. 12. Experimental setup for the production of Bragg gratings in optical fiber by UV irradiation interferometer method.

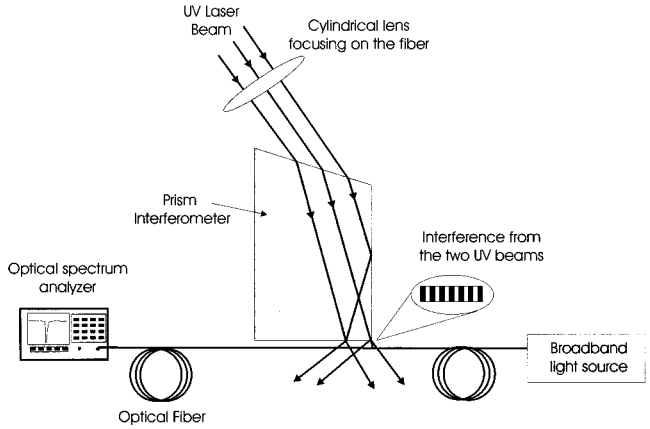

FIG. 13. Schematic of prism interferometer for fabricating Bragg gratings.

(derived in Sec. IV) states that the Bragg resonance wavelength, λ_B, in the core of the fiber is twice the product of the effective core index, n, and the period of the grating. Hence, a Bragg grating resonance wavelength can be represented in terms of the UV writing wavelength and the half-angle between intersecting UV beams as

$$\lambda_B = \frac{n\lambda_w}{\sin \varphi}. \tag{3.2}$$

From Eq. (3.2) one can easily see that the Bragg grating wavelength can be varied either by changing λ_w and/or φ. The choice of λ_w is limited to the UV photosensitivity region of the fiber, however, there is no restriction set on the choice of the angle φ.

The most important advantage offered by the amplitude-splitting interferometric fabrication technique is the ability to inscribe Bragg gratings at any wavelength. This is accomplished by simply changing the intersecting angle between the UV beams. This method also offers complete flexibility for producing gratings of various lengths, which allows the fabrication of wavelength narrowed or broadened gratings. Furthermore, unique grating geometries, such as linearly chirped gratings, can be produced by using curved reflecting surfaces in the beam delivery path.

The main disadvantage of the amplitude-splitting interferometric technique is its susceptibility to mechanical vibrations. Displacements as small as submicrons in the position of mirrors, beam splitter, or mounts in the interferometer can cause the fringe pattern to drift, washing out the grating. Furthermore, due to long separate optical path lengths involved in the interferometers, air currents, which affect the refractive index locally, may cause a problem in the formation of a stable fringe pattern. In addition to the above shortcomings, quality gratings can only be produced with a laser source that has good spatial and temporal coherence with excellent output power stability.

(b) *Wave-front-splitting interferometers.* Wave-front-splitting interferometers are not as popular as the amplitude-splitting interferometers for grating fabrication. However, they have some useful advantages over the amplitude-splitting interferometers. Two such wave-front-splitting interferometers that have been used to fabricate Bragg gratings in optical fibers are the prism interferometer[45,46] and the Lloyd's interferometer.[47]

A schematic of the prism interferometer used in fabricating Bragg grating is shown in Fig. 13. The prism is made from high homogeneity ultraviolet-grade fused silica allowing for good transmission characteristics. In this setup, the UV beam is expanded laterally by refraction at the input face of the prism. The expanded beam is spatially bisected by the prism edge, and half of the beam is spatially reversed by total internal reflection from the prism face. The two half-beams are then recombined at the output face of the prism, giving a fringe pattern parallel to the photosensitive fiber core. A cylindrical lens placed just before the setup helps in forming the interference pattern on a line along the fiber core.

The experimental setup for fabricating gratings with the Lloyd interferometer is shown in Fig. 14. This interferometer consists of a dielectric mirror, which directs half of the UV beam to a fiber that is perpendicular to the mirror. The UV beam is centered at the intersection of the mirror surface and fiber. The overlap of the direct and deviated portions of UV beam creates interference fringes normal to the fiber axis. As in the case of the previous interferometers, a cylindrical lens is usually placed in front of the system to focus the fringe pattern along the core of the fiber.

A key advantage of the wave-front-splitting interfero-

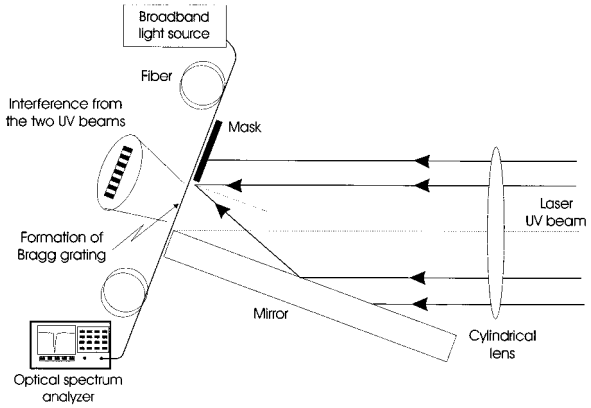

FIG. 14. Schematic of Lloyd interferometer for fabricating Bragg gratings.

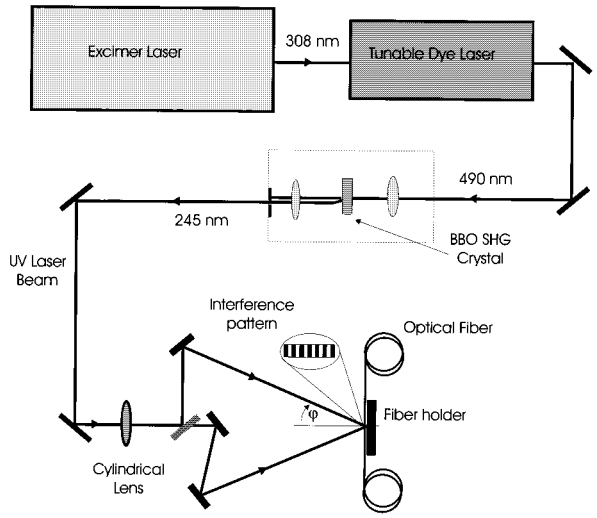

FIG. 15. Experimental setup of an excimer pump dye laser with a frequency doubled BBO crystal for generating UV light at 245 nm for inscribing Bragg gratings in an interferometer.

meters is that only one optical component is used. This greatly reduces the sensitivity to mechanical vibrations. In addition, the short distance where the UV beams are separated reduces the wave-front distortion induced by air currents and temperature differences between the two interfering beams. Furthermore, this assembly can be rotated easily to vary the angle of intersection of the two beams for wavelength tuning. One disadvantage of this system is the limitation on the grating length, which is restricted to half of the beam width. Another disadvantage is the range of Bragg wavelength tunability, which is restricted by the physical arrangement of the interferometers. That is, as the intersection angle increases, the difference between beam path lengths increases. Therefore, the beam coherence length limits the Bragg wavelength tunability.

(c) *Laser source requirements.* Laser sources used for inscribing Bragg gratings via the above interferometric techniques must have good temporal and spatial coherence. The spatial coherence requirements can be relaxed in the case of the amplitude-split interferometer by simply making sure that the total number of reflections are the same in both arms. This is especially critical in the case where a laser with low spatial coherence, like an excimer laser, is used as the source of UV light. The temporal coherence has to be at least the length of the grating in order for the interfering beams to have a good contrast ratio, thus, resulting in good quality Bragg gratings. The above coherence requirement together with the UV wavelength range needed (240–250 nm) forced researchers to initially use very complicated laser systems.

One such system consists of an excimer pumped tunable dye laser, operating in the range of 480–500 nm. The output from the dye laser is focused on a nonlinear crystal to double the frequency of the fundamental light (Fig. 15). Typically, this arrangement provides 10–20 ns pulses (depending on the excimer pump laser), approximately, 3–5 mJ with excellent temporal and spatial coherence. An alternative to this elaborate and often troublesome setup is a specially designed excimer laser that has a long temporal coherence length.

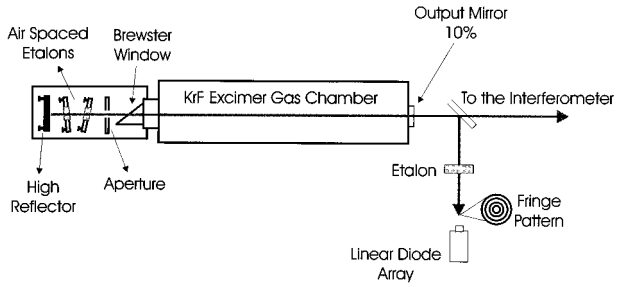

FIG. 16. Experimental arrangement of for narrowing the linewidth of an excimer laser (after Ref. 48).

These spectrally narrow linewidth excimer lasers may operate for extended periods of time on the same gas mixture with little changes in their characteristics. Commercially available narrow linewidth excimer systems are complicated oscillator amplifier configurations, which make them extremely costly. Othonos and Lee[48] developed a low-cost simple technique where existing KrF excimer lasers may be retrofitted with a spectral narrowing system for inscribing Bragg gratings in a side written interferometric configuration. In that work, a commercially available KrF excimer laser (Lumonics Ex-600) was modified to produce a spectrally narrow laser beam (Fig. 16) with a linewidth of approximately 4×10^{-12} m. This system was used to successfully inscribe Bragg gratings in photosensitive optical fibers.[48]

An alternative to the above system, which is becoming very popular is the intracavity frequency-double argon ion laser[49] that uses beta-barium borate (BBO). This system efficiently converts high-power visible laser wavelengths into deep ultraviolet (244 and 248 nm). The characteristics of these lasers include unmatched spatial coherence, narrow linewidth and excellent beam pointing stability, which make such systems very successful in inscribing Bragg gratings in optical fibers.[49]

2. Phase mask technique

One of the most effective methods for inscribing Bragg gratings in photosensitive fiber is the phase-mask technique.[50,51] This method employs a diffractive optical element (phase mask) to spatially modulate the UV writing beam (see Fig. 17). Phase masks may be formed holographically or by electron-beam lithography.[52] Holographically induced phase masks have no stitch error, which is normally present in the electron-beam phase masks.[53] However, complicated patterns can be written into the electron beams fabricated masks (quadratic chirps, Moire patterns, etc.). The phase-mask grating has a one-dimension surface-relief structure fabricated in a high-quality fused silica flat transparent to the UV writing beam. The profile of the periodic gratings is chosen such that when an UV beam is incident on the phase mask, the zero-order diffracted beam is suppressed to less than a few percent (typically, less than 5%) of the transmitted power. In addition, the diffracted plus and minus first orders are maximized; each containing, typically, more than 35% of the transmitted power. A near-field fringe pattern is produced by the interference of the plus and

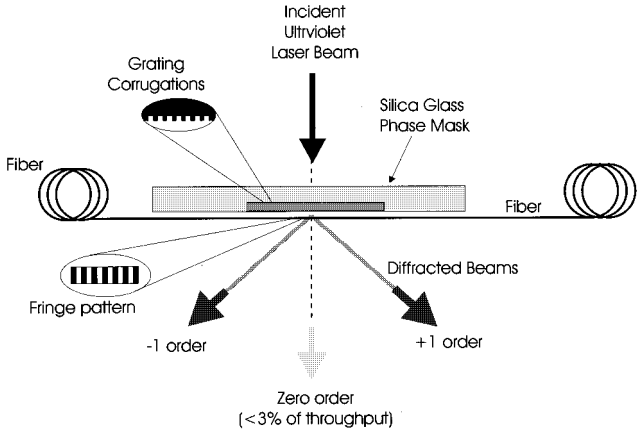

FIG. 17. Schematic of the phase-mask technique for photoimprinting a refractive-index Bragg grating in a photosensitive optical fiber.

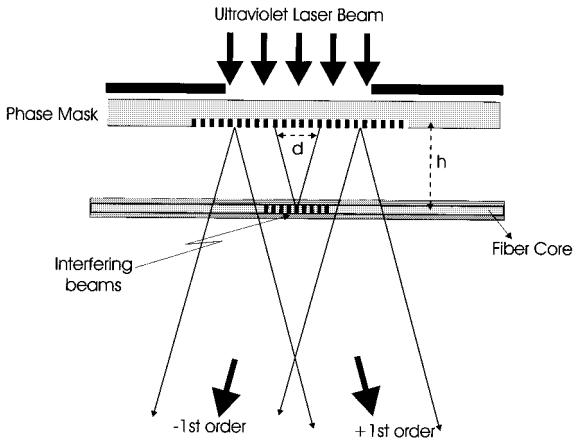

FIG. 18. Schematic of the phase-mask geometry for inscribing Bragg grating in optical fibers. The plus and minus first-order diffracted beams interfere at the fiber core, placed at a distance h from the mask.

minus first-order diffracted beams. The period of the fringes are one-half that of the mask. The interference pattern photoimprints a refractive-index modulation in the core of a photosensitive optical fiber placed in contact with or in close proximity immediately behind the phase mask (Fig. 17). A cylindrical lens may be used to focus the fringe pattern along the fiber core.

The phase mask greatly reduces the complexity of the fiber grating fabrication system. The simplicity of using only one optical element provides a robust and an inherently stable method for reproducing fiber Bragg gratings. Since the fiber is usually placed directly behind the phase mask in the near field of the diffracting UV beams, sensitivity to mechanical vibrations and, therefore, stability problems are minimized. Low temporal coherence does not effect the writing capability (as opposed to the interferometric technique) due to the geometry of the problem.

KrF excimer lasers are the most common UV sources used to fabricate Bragg gratings with a phase mask. The UV laser sources, typically, have low spatial and temporal coherence. The low spatial coherence requires the fiber to be placed in near contact to the grating corrugations on the phase mask in order to induce maximum modulation in the index of refraction. The further the fiber is placed from the phase mask, the lower the induced index modulation, resulting in lower reflectivity Bragg gratings. Clearly, the separation of the fiber from the phase mask is a critical parameter in producing quality gratings. However, placing the fiber in contact with the fine grating corrugations is not desirable due to possible damage to the phase mask. Othonos and Lee[54] demonstrated the importance of spatial coherence of UV sources used in writing Bragg gratings using the phase-mask technique. Improving the spatial coherence of the UV writing beam not only improves the strength and quality of the gratings inscribed by the phase-mask technique, it also relaxes the requirement that the fiber has to be in contact with the phase mask.

To understand the significance of spatial coherence in the fabrication of Bragg grating using the phase-mask technique, it is helpful to consider a simple schematic diagram (see Fig. 18). Consider the fiber core to be at a distance h from the phase mask. The transmitted *plus* and *minus* first orders that interfere to form the fringe pattern on the fiber emanate from different parts of the mask (referred to as distance d in Fig. 18). Since the distance of the fiber from the phase mask is identical for the two interfering beams, the requirement for temporal coherence is not critical for the formation of a high contrast fringe pattern. On the other hand, as the distance h increases, the separation d between the two interfering beams emerging from the mask, increases. In this case, the requirement for good spatial coherence is critical for the formation of a high contrast fringe pattern. As the distance h extends beyond the spatial coherence of the incident UV beam, the interference fringe contrast will deteriorate, eventually resulting in no interference at all. The importance of spatial coherence was also demonstrated by Dyer *et al.*[55] who used a KrF laser irradiated phase mask to form gratings in polyimide film.

One of the advantages of not having to position the fiber against the phase mask is the freedom to be able to angle the fiber relative to the mask forming blazed gratings. Placing one end of the exposed fiber section against the mask and the other end at some distance form the mask, it is possible to change the induced Bragg grating center wavelength. From simple geometry (see the inset in Fig. 19), one can derive a general expression for the tunability of the Bragg grating center wavelength, given by

$$\lambda_B = 2n\Lambda \sqrt{1+\left(\frac{r}{l}\right)^2}, \tag{3.3}$$

where Λ is the period of the fiber grating, r is the distance from one end of the exposed fiber section to the phase mask, and l is the length of the phase grating. For a fixed phase-mask period changing r will result in blazed gratings with changing center Bragg wavelength. In the experiments described in Ref. 54, a phase mask with $\Lambda = 0.531\ \mu$m ($l = 10\,000\ \mu$m) was utilized resulting in $\lambda_B = 1.5580\ \mu$m at $r = 0$ (the fiber placed parallel to the phase mask). Figure 19 shows the theoretical curve for the tunability of the inscribed Bragg grating as a function of distance r. The experimental values for the peak reflectivities of the Bragg gratings are also shown for different r values.

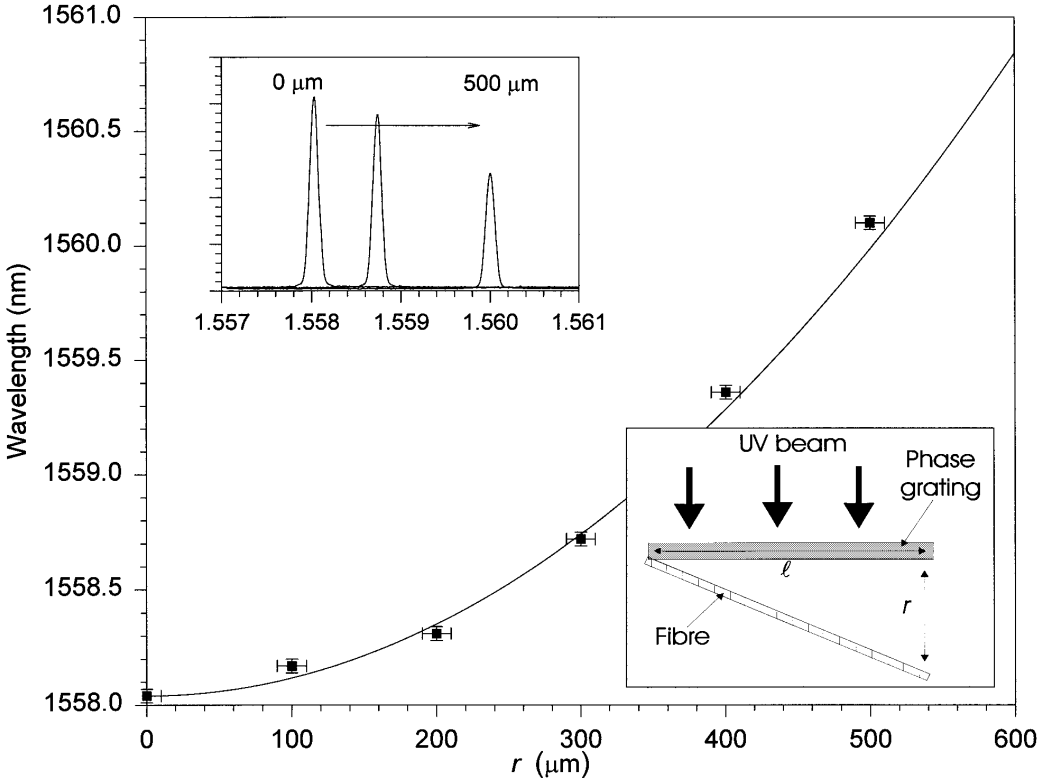

FIG. 19. Experimental result of tuning a Bragg grating by tilting the writing fiber.

A variation to the phase-mask scheme with the fiber in near contact to the mask (as described above) has been demonstrated.[56] This technique is based on an UV transmitting silica prism. The -1 and $+1$ orders are internally reflected within a rectangular prism as shown in Fig. 20 and interfere at the fiber. This noncontact technique is flexible and allows quick changes of the inscribed Bragg wavelength.

3. Point-by-point fabrication of Bragg gratings

The point-by-point technique[57] for fabricating Bragg gratings is accomplished by inducing a change in the index of refraction a step at a time along the core of the fiber. Each grating plane is produced separately by a focused single pulse from an excimer laser. A single pulse of UV light from an excimer laser passes through a mask containing a slit. A focusing lens images the slit onto the core of the optical fiber from the side, as shown in Fig. 21, and the refractive index of the core in the irradiated fiber section increases locally. The fiber is then translated through a distance Λ corresponding to the grating pitch in a direction parallel to the fiber axis and the process is repeated to form the grating structure in the fiber core. Essential to the point-by-point fabrication technique is a very stable and precise submicron translational system.

The main advantage of the point-by-point writing technique lies in its flexibility to alter the Bragg grating parameters. Because the grating structure is built up a point at a time, variations in grating length, grating pitch, and spectral

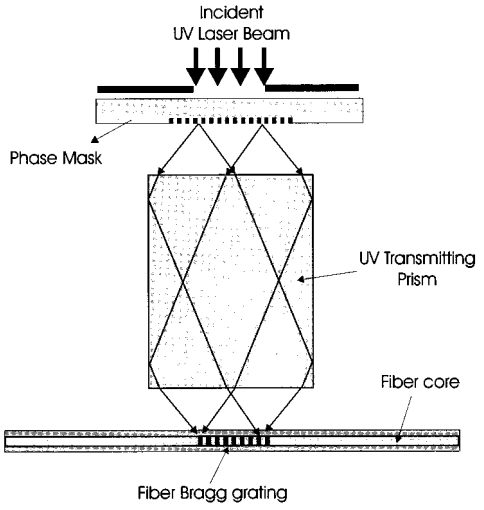

FIG. 20. Noncontact technique interferometric phase-mask technique for generating fiber Bragg gratings.

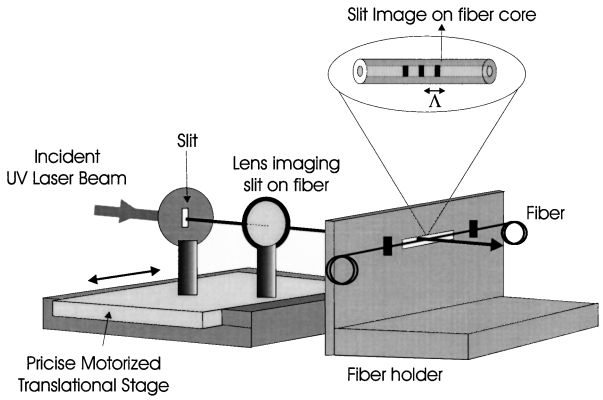

FIG. 21. Setup for point-by-point grating fabrication.

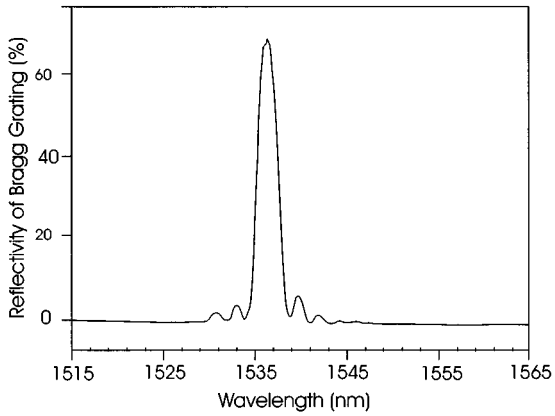

FIG. 22. Reflection spectrum of a third-order Bragg grating fabricated using the point-by-point method (after Ref. 57).

response can easily be incorporated. Chirped gratings can be produced accurately simply by increasing the amount of fiber translation each time the fiber is irradiated. The point-by-point method allows for the fabrication of spatial-mode converters[58] and polarization-mode converters or rocking filters[59] that have grating periods, Λ, ranging from tens of micrometers to tens of millimeters. Because the UV pulse energy can be varied between points of induced index change, the refractive-index profile of the grating can be tailored to provide any desired spectral response.

One disadvantage of the point-by-point technique is that it is a tedious process. Because it is a step-by-step procedure, this method requires a relatively long process time. Errors in the grating spacing due to thermal effects and/or small variations in the fiber's strain can occur. This limits the gratings to a very short length. Typically, the grating period required for first-order reflection at 1550 nm is approximately 530 nm. Because of the submicron translation and tight focusing required, first-order 1550 nm Bragg gratings have yet to be demonstrated using the point-by-point technique. Malo *et al.*[57] have only been able to fabricate Bragg gratings that reflect light in the second and third order, which have a grating pitch of approximately 1 and 1.5 μm, respectively. Figure 22 shows the reflection spectrum of the third-order Bragg grating fabricated using the point-by-point method. This third-order grating is made up of 225 index perturbations with grating period Λ, of 1.59 μm resulting in a grating length of 360 μm. The grating has a peak reflectivity of 70% at 1536 nm and a full width at half-maximum of 2.7 nm.

4. Mask image projection

In addition to the above well-known techniques for fabricating fiber Bragg gratings, high-resolution mask projection has been demonstrated[60] as a means of inscribing Bragg gratings in optical fiber using excimer laser pulses. The mass projection system consists of a excimer laser source generating an UV beam, which is incident on a transmission mask. In Mihailov and Gower's[60] experiments, the transmission mask consisted of a series of UV opaque line spaces. The transmitted beam was imaged onto the fiber core by a multicomponent fused silica high-resolution system having a demagnification of 10:1. In their work, gratings with periods of

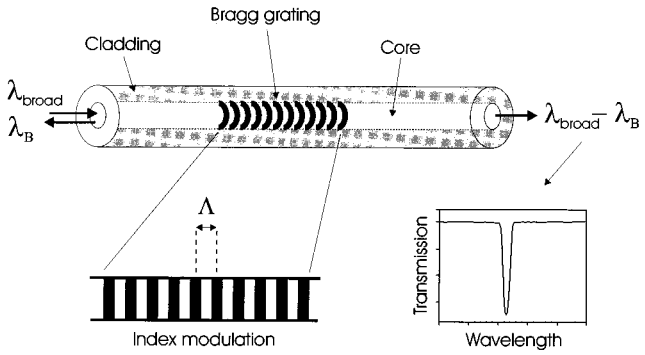

FIG. 23. Illustration of a uniform Bragg grating with constant index modulation amplitude and period. Also shown are the incident, diffracted, and grating wave vectors that have to match for momentum to be conserved.

1, 2, 3, 4, and 6 μm have been written in single-mode Ge-doped fiber using mask-imaging techniques. Because of the simplicity of the source and setup, the recording of coarse period gratings by mask-imaging exposures, in some cases, may be more flexible than other techniques. Complicated grating structures (blazed, chirped, etc.) can be readily fabricated with this method by implementing a simple change of mask.

IV. FIBER BRAGG GRATINGS

A. Properties of Bragg gratings

In its simplest form, a fiber Bragg grating consists of a periodic modulation of the index of refraction in the core of a single-mode optical fiber. These types of uniform fiber gratings, where the phase fronts are perpendicular to the fiber longitudinal axis and the grating planes are of a constant period (Fig. 23), are considered the fundamental building blocks for most Bragg grating structures. Light guided along the core of an optical fiber will be scattered by each grating plane. If the Bragg condition is not satisfied, the reflected light from each of the subsequent planes becomes progressively out of phase and will eventually cancel out. Where the Bragg condition is satisfied, the contributions of reflected light from each grating plane add constructively in the backward direction to form a back-reflected peak with a center wavelength defined by the grating parameters.

The Bragg grating condition is simply the requirement that satisfies both energy and momentum conservation. Energy conservation ($\hbar\omega_f = \hbar\omega_i$) requires that the frequency of the incident radiation and the reflected radiation is the same. Momentum conservation requires that the incident wave vector, $\mathbf{k}_i$, plus the grating wave vector, $\mathbf{K}$, equal the wave vector of the scattered radiation $\mathbf{k}_f$, this is simply stated as

$$\mathbf{k}_i + \mathbf{K} = \mathbf{k}_f, \tag{4.1}$$

where the grating wave vector, $\mathbf{K}$, has a direction normal to the grating planes and it has a magnitude $2\pi/\Lambda$ (Λ is the grating spacing shown in Fig. 23). The diffracted wave vector is equal in magnitude but opposite in direction to the incident wave vector. Hence, the momentum conservation condition becomes

$$2\left(\frac{2\pi n}{\lambda_B}\right)=\frac{2\pi}{\Lambda}, \tag{4.2}$$

which simplifies to the first-order Bragg condition

$$\lambda_B=2n\Lambda, \tag{4.3}$$

where the Bragg grating wavelength, λ_B, is the free-space-center wavelength of the input light that will be back reflected from the Bragg grating, and n is the effective refractive index of the fiber core at the free-space-center wavelength. Some of the properties such as reflectivity and bandwidth of the simplest type of grating, namely the uniform Bragg grating, will be discussed below.

1. Uniform Bragg grating reflectivity

Consider a uniform Bragg grating formed within the core of an optical fiber with an average refractive index n_0. The index of refractive profile can be expressed as

$$n(x)=n_0+\Delta n\ \cos\left(\frac{2\pi x}{\Lambda}\right), \tag{4.4}$$

where Δn is the amplitude of the induced refractive-index perturbation (typically, 10^{-5}–10^{-2}) and x is the distance along the fiber longitudinal axis. Using the coupled-mode theory analytical description of the reflection properties of Bragg gratings may be obtained.[7] The reflectivity of a grating with constant modulation amplitude and period is given by the following expression:

$$R(l,\lambda)=\frac{\Omega^2\ \sinh^2(sl)}{\Delta k^2\ \sinh^2(sl)+s^2\ \cosh^2(sl)}, \tag{4.5}$$

where $R(l,\lambda)$ is the reflectivity, which is a function of the grating length l, and wavelength λ. Ω is the coupling coefficient, $\Delta k=k-\pi/\lambda$ is the detuning wave vector, $k=2\pi n_0/\lambda$ is the propagation constant, and, finally, $s=\sqrt{\Omega^2-\Delta k^2}$. The coupling coefficient, Ω, for the sinusoidal variation of index perturbation along the fiber axis is given by

$$\Omega=\frac{\pi\Delta n\,\eta(V)}{\lambda}, \tag{4.6}$$

where $\eta(V)\approx 1-1/V^2$, $V\geqslant 2.4$. This η is a function of the fiber parameter V that represents the fraction of the integrated fundamental-mode intensity contained in the core. At the Bragg grating center wavelength, there is no wave-vector detuning and $\Delta k=0$, therefore, the expression for the reflectivity becomes

$$R(l,\lambda)=\tanh^2(\Omega l). \tag{4.7}$$

The reflectivity increases as the induced index of refraction change increases. Similarly, as the length of the grating increases so does the resultant reflectivity. A calculated reflection spectrum as a function of the wavelength detuning is shown in Fig. 24. The side lobes of the resonance are due to multiple reflections to and from opposite ends of the grating region.

A general expression for the approximate full width at half-maximum bandwidth of a grating is given by[9]

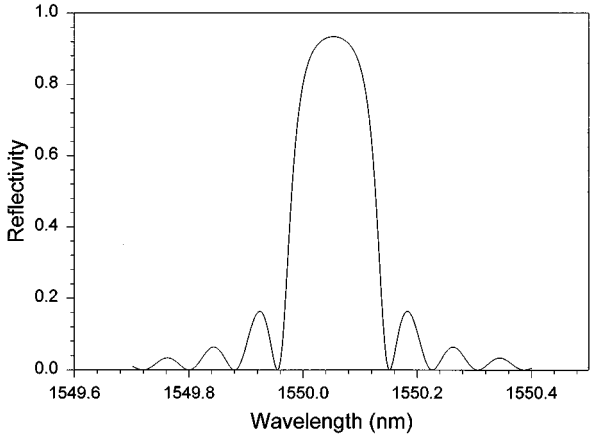

FIG. 24. Bragg grating reflection spectrum as a function of wavelength detuning.

$$\Delta\lambda=\lambda_B\alpha\sqrt{\left(\frac{\Delta n}{2n_0}\right)^2+\left(\frac{1}{N}\right)^2}, \tag{4.8}$$

where N is the number of the grating planes. The parameter α is ~ 1 for strong gratings (for grating with near 100% reflection) whereas $\alpha\sim 0.5$ for weak gratings.

2. Strain and temperature sensitivity of Bragg gratings

The Bragg grating resonance, which is the center wavelength of light back reflected from a Bragg grating depends on the effective index of refraction of the core and the periodicity of the grating. The effective index of refraction, as well as the periodic spacing between the grating planes, will be affected by changes in strain and temperature. Using Eq. (4.3), the shift in the Bragg grating center wavelength due to strain and temperature changes is given by

$$\Delta\lambda_B=2\left(\Lambda\ \frac{\partial n}{\partial l}+n\ \frac{\partial\Lambda}{\partial l}\right)\Delta l+2\left(\Lambda\ \frac{\partial n}{\partial T}+n\ \frac{\partial\Lambda}{\partial T}\right)\Delta T. \tag{4.9}$$

The first term in Eq. (4.9) represents the strain effect on an optical fiber. This corresponds to a change in the grating spacing and the strain-optic induced change in the refractive index. The above strain effect term may be expressed as[61]

$$\Delta\lambda_B=\lambda_B(1-p_e)\epsilon_z, \tag{4.10}$$

where p_e is an effective strain-optic constant defined as

$$p_e=\frac{n^2}{2}\left[p_{12}-\nu(p_{11}+p_{12})\right], \tag{4.11}$$

where p_{11} and p_{12} are components of the strain-optic tensor, n is the index of the core, and ν is the Poisson's ratio. For a typical optical fiber $p_{11}=0.113$, $p_{12}=0.252$, $\nu=0.16$, and $n=1.482$. Using these parameters and the above equations, the expected sensitivity at ~ 1550 nm is a 1.2 pm change as a result of applying 1 $\mu\epsilon$ to the Bragg grating. Experimental results of a Bragg center wavelength shift with applied stress on a 1548.2 nm grating are shown in Fig. 25.

The second term in Eq. (4.9) represents the temperature effect on an optical fiber. A shift in the Bragg wavelength

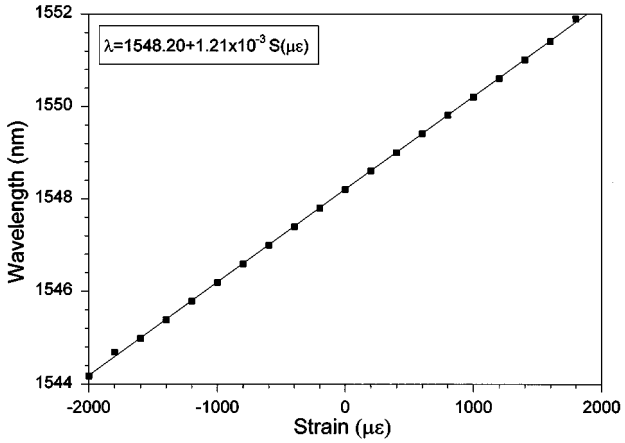

FIG. 25. Bragg grating wavelength as a function of applied stress for a 1548.2 nm grating. The Bragg grating was the output coupler of an erbium-doped fiber laser.

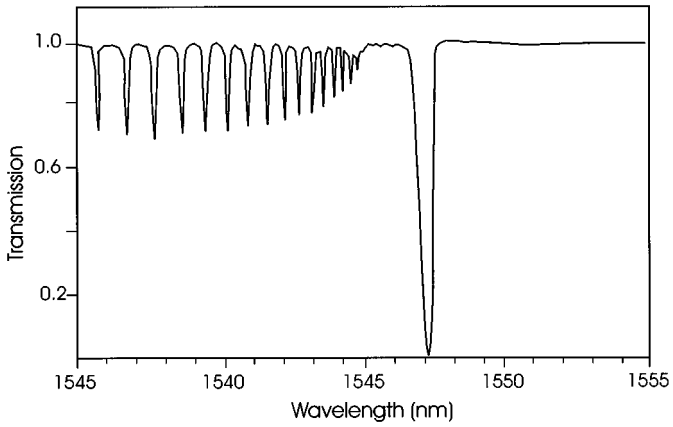

FIG. 27. Schematic of transmission profile for a strong fiber Bragg grating showing loss to radiation modes on the short-wavelength side, sharply modified by the cladding-modes structure.

due to thermal expansion changes the grating spacing and changes the index of refraction. This fractional wavelength shift for a temperature change ΔT may be written as[61]

$$\Delta\lambda_B=\lambda_B(\alpha+\zeta)\Delta T, \tag{4.12}$$

where $\alpha=(1/\Lambda)(\partial\Lambda/\partial T)$ is the thermal expansion coefficient for the fiber (approximately, 0.55×10^{-6} for silica). The quantity $\zeta=(1/n)(\partial n/\partial T)$ represents the thermo-optic coefficient and it is approximately equal to 8.6×10^{-6} for the germania-doped silica core fiber. Clearly, the index change is by far the dominant effect. From Eq. (4.12), the expected sensitivity at a $\sim$1550 nm Bragg grating is approximately 13.7 pm/C. Figure 26 shows experimental results of a Bragg grating center wavelength shift as a function of temperature.

3. Cladding and radiation-mode coupling

Bragg gratings written in a highly photosensitive fiber, such as, fiber which has been hydrogenated, have a very pronounced transmission structure on the short-wavelength side of the Bragg peak (see Fig. 27).[62] This feature is only observable in the transmission spectrum (viewed in reflection, only the main peak appears), therefore, this structure must be due to light leaving the fiber from the side, and to analyze it one must take into account radiation-mode coupling. Usually, radiation-mode coupling, which is routinely observed from surface relief gratings made by physically etching the core in a polished optical fiber, is a smooth function of the wavelength. However, the transmission spectrum of the Bragg grating (as seen in Fig. 27) consists of multiple sharp peaks that modulate this coupling, and it is a direct consequence of the cylindrical cladding-air interface. This effect may be eliminated by dipping the cladding into glycerin, which in effect eliminates the cladding-air interface. Nevertheless, the cladding-mode radiation-related problems become very serious with large excess losses at wavelengths shorter than the peak reflection wavelength. As a result, highly reflective chirped gratings have lower reflectivity at shorter wavelengths when the signal is coupled form the longer-wavelength side of the fiber grating. There are several approaches to avoiding the radiation-mode effect. One proposed method to counter this problem is based on suppression of the normalized refractive-index modulation for this coupling by having a uniform photosensitive region across the cross-section plane of the optical fiber.[63] From the orthogonality principle of the modes, the overlap of the modal fields and the grating-index modulation would be zero in this case. The LP_{01} mode will, therefore, not couple into any of the cladding modes. Since the LP_{01} mode only has a significant filed distribution over the core and the part of the cladding immediately next to the core, it is usually sufficient to have only this part of the optical fiber photosensitive. Although it is possible to introduce a photosensitive cladding around a photosensitive core, it is, however, very difficult to obtain the same photosensitivity over both cladding and core. The second proposed method is to use a high NA fiber.[64] The use of a high NA fiber increases the gap between the main grating band and the next cladding-mode coupling band, so it leaves a useful operating band. However, such a band is only approximately 7 nm wide in a high-NA fiber, and this is much less than what is desired in most applications.

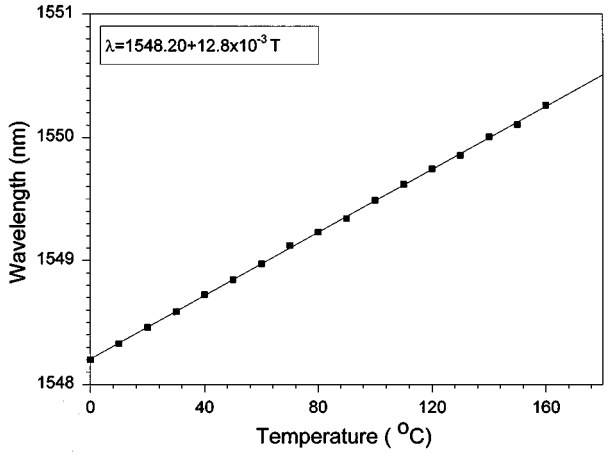

FIG. 26. Bragg grating wavelength as a function of temperature change for a 1548.2 nm grating. The Bragg grating was the output coupler of an erbium-doped fiber laser.

Recently, Dong and co-workers[65] proposed and demonstrated a method for suppressing the coupling from guided optical modes into cladding modes. A depressed cladding is

added between the photosensitive core and the normal cladding. Such a depressed cladding is very effective in reducing the cladding-mode field strength over the core region of the optical fiber and, therefore, reduces the coupling strength between the guided mode to the cladding modes. By introducing a depressed cladding with appropriate index and thickness, substantial suppression of the coupling into the cladding modes can be achieved. This method can also be combined with the photosensitive cladding method to achieve a further suppression of the coupling.

B. Types of fiber Bragg gratings

There are several distinct types of fiber Bragg grating structures such as the common *Bragg reflector*, the *blazed Bragg grating*, and the *chirped Bragg grating*. These fiber Bragg gratings are distinguished either by their grating pitch (spacing between grating planes) or tilt (angle between grating planes and fiber axis). The most common fiber Bragg grating is the *Bragg reflector*, which has a constant pitch. The *blazed grating* has phase fronts tilted with respect to the fiber axis, that is, the angle between the grating planes and the fiber axis is less than 90°. The *chirped grating* has an aperiodic pitch, that is, a monotonic increase in the spacing between grating planes. A brief overview of these Bragg gratings along with some of their applications will be presented. In addition, a description of what is commonly referred to as *type II gratings*, as well as some novel *Bragg grating structures* will be given below.

1. Common Bragg reflector

The *common Bragg reflector* was the first intracore fiber grating inscribed using the ''self-induced'' writing method. This simplest and most used fiber Bragg gratings are illustrated in Fig. 23.

Depending on the parameters such as grating length and magnitude of induced index change, the Bragg reflector can function as a narrow-band transmission or reflection filter or a broadband mirror. In combination with other Bragg reflectors, these devices can be arranged to function as bandpass filters. Two such configurations are shown in Fig. 28.

Bragg reflectors are considered as excellent strain and temperature sensing devices because the measurements are wavelength encoded. This eliminates the problems of amplitude or intensity fluctuations that exist in many other types of fiber sensors. Since each Bragg reflector can be designated with its own wavelength-encoded signature, a series of these gratings can be written on the same fiber, each having a distinct Bragg resonance signal. This configuration can be used for wavelength division multiplexing or quasidistributed sensing.[66] These gratings have also been demonstrated to be very useful components in tunable fiber or semiconductor lasers.[67–69] It serves as one or both ends of the laser cavity, depending on the laser configuration, and it tunes the laser wavelength by varying the Bragg resonance feedback signal. Ball and Morey[70] demonstrated a continuously tunable single-mode erbium fiber laser. In their laser system, two Bragg reflectors were used in a Fabry–Perot configuration. Continuous tunability, without mode hopping, was achieved when both the gratings and enclosed fiber were stretched uniformly.

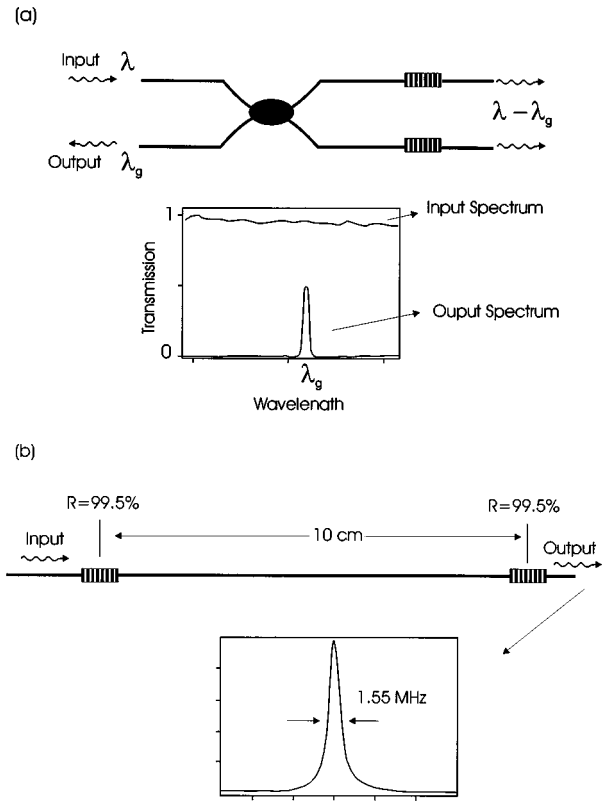

FIG. 28. Fiber-optic bandpass filters using Bragg reflectors. (a) filter arranged in a Michelson-type configuration, and (b) filter arranged in a Fabry–Perot-type configuration.

Bragg grating fiber lasers can also be used as sensors where the Bragg reflector serves the dual purpose of tuning element and sensor.[71] A series of Bragg reflectors having distinct wavelength-encoded signatures can be multiplexed in a fiber laser sensor configuration for multipoint sensing.[72,73]

2. Blazed Bragg gratings

Tilting (or blazing) the Bragg grating planes at angles to the fiber axis (Fig. 29) will result in light that is otherwise guided in the fiber, to be coupled out of the fiber core into loosely bound guided cladding modes or into radiation modes outside the fiber. The tilt of the grating planes and strength of the index modulation determines the coupling efficiency and bandwidth of the light that is tapped out.

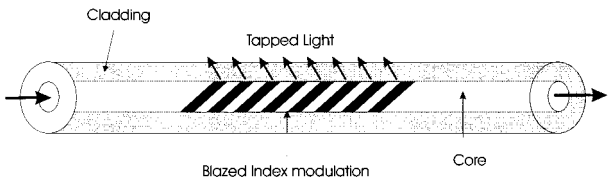

FIG. 29. Schematic diagram of a blazed grating. Light is directed either upward or downward depending on the propagation direction of the bound mode.

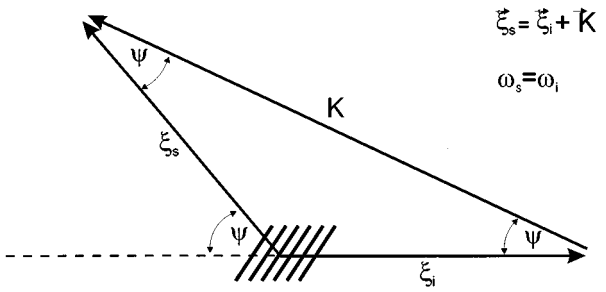

FIG. 30. Vector diagram for the Bragg condition of a blazed grating. The magnitude of the incident ξ_i and scattered, ξ_s, wave vector are the same.

The criterion to satisfy the Bragg condition of a blazed grating is similar to that of the Bragg reflector that was analyzed earlier. Figure 30 illustrates the vector diagram of the Bragg condition (energy and momentum conservation) for the blazed grating. Here, the wave vector of the grating is incident at an angle, ψ, with respect to the fiber axis. The magnitudes of the incident ξ_i and the scattered ξ_s, wave vectors must be equal ($\xi = \xi_i = \xi_s$). Simple trigonometry shows that the scattered wave vector must be at an angle 2ψ with respect to the fiber axis. Applying the law of cosines to the momentum diagram gives

$$\xi_i^2 + \xi_s^2 - 2\xi_i\xi_s \cos(\pi - 2\psi) = K^2, \tag{4.13}$$

which reduces to $\cos(\psi) = K/2\xi$ and shows that the scattering angle is restricted by the Bragg wavelength and the effective refractive index. It is clear from Eq. (4.13) that, for blazed gratings, not only different wavelengths emerge at different angles, but different modes of the same wavelength also emerge at slightly different angles due to their different propagation constants. Figure 31 shows the output coupling of 488 and 514.5 nm light from an argon ion laser. The green argon ion wavelength has two modes and the blue wavelength has three modes, which propagate in the fiber. These wavelengths, as well as their modes, are well separated and resolvable, thus, the grating tap acts as a spectrometer and mode discriminator. Meltz and Morey[74] have achieved outcoupling efficiencies as high as 21% at 488 and 514.5 nm.

Erbium-doped fiber amplifiers are now an integral part of long-haul high-bit-rate communication systems and are finding applications in areas of wide bandwidth amplification. Kashyap *et al.*[75] demonstrated the use of multiple blazed gratings to flatten the gain spectrum of erbium-doped fiber amplifiers. A gain variation of ± 1.6 dB over a bandwidth of 33 nm in a saturated erbium-doped fiber amplifier

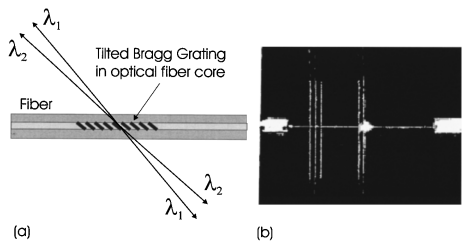

FIG. 31. Illustration of separated wavelength tapped out at different angles. Image of the radiation out-coupled at the 488 and 514.5 nm from a fiber Bragg grating tap. From Meltz and Morey (after Ref. 74).

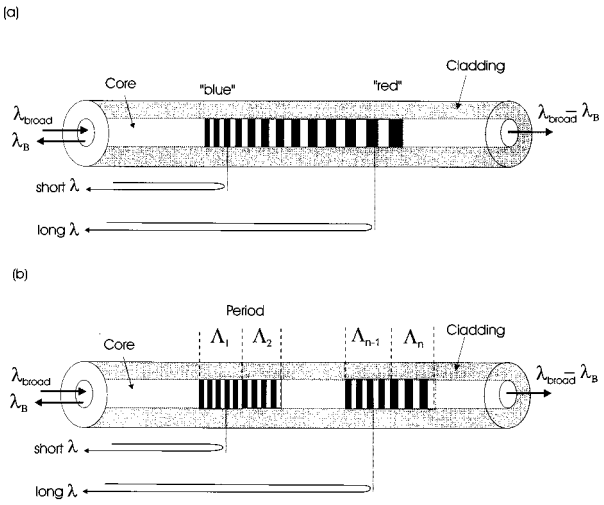

FIG. 32. Schematic diagram of a chirped grating with an aperiodic pitch (a). For forward propagating light as shown, longer wavelengths travel further into the grating before being reflected. A schematic diagram of a cascade of several gratings with increasing period, which are used to simulate long chirped gratings (b).

was reduced to ± 0.3 dB. This is important in fiber communications that use several signals at different wavelengths.

Another interesting application of blazed gratings is in mode conversion. Mode converters are fabricated by inducing a periodic refractive-index perturbation along the fiber length with a periodicity that bridges the momentum mismatch between the modes to allow phase-matched coupling between the selected modes. Different grating periods are used for mode conversion at different wavelengths. Hill *et al.*[59] demonstrated efficient mode conversion between forward propagation LP_{01} and LP_{11} modes.

3. Chirped Bragg grating

A chirped Bragg grating is a grating that has a monotonically varying grating period, Fig. 32. This can be realized by axially varying either the period of the grating Λ or the index of refraction of the core or both. Chirped gratings have been written in optical fibers using various methods.[76–80] A double exposure technique has been used by Hill *et al.*[79] in forming a 1.5 cm long chirped grating. The effective mode index of the waveguide was modulated linearly over the grating length with radiation from an excimer laser and then the same length was reexposed with a phase mask to produce a linearly chirped grating. A chirp of 0.4 nm was demonstrated at 1549 nm. The delay induced by the gratings was shown to be approximately 120 ps over the entire bandwidth of the grating.

A highly repeatable and simple technique for producing chirped gratings is based on the phase mask where the linear chirp is approximated by a step chirp. In this technique, a cascade of several gratings with increasing period are used to simulate a long chirped grating shown in Fig. 32(b). The chirped structure is initially inscribed on the phase mask and then the mask is used to fabricate the chirped Bragg gratings in the photosensitive fiber. Clearly, this is a highly repeatable and controllable technique for producing any type of chirped Bragg structure in fiber.

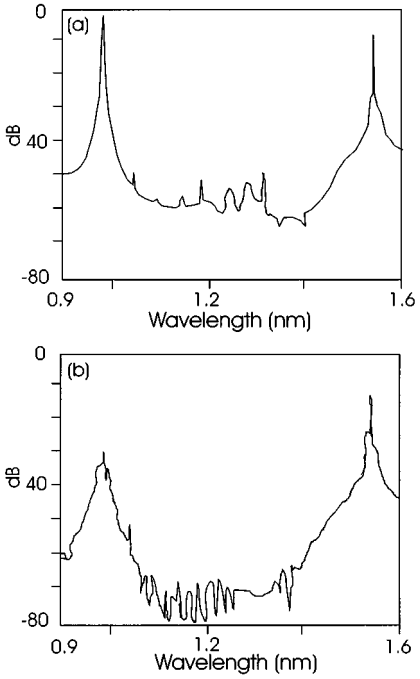

FIG. 33. Emission spectrum from a fiber amplifier (a) without and (b) with a broadband chirped fiber Bragg filter (after Ref. 83).

With the introduction of an erbium-doped amplifier in long-haul high-bit-rate communication systems, the main limitation in transmitting over such distance is the pulse broadening caused by chromatic dispersion. Dispersion-induced pulse broadening can be eliminated by an element having a dispersion of opposite sign and equal magnitude to that of the optical fiber link. In a chirped grating, the resonant frequency is a linear function of the axial position along the grating so that different frequencies, present in the pulse, are reflected at different points and, thus, acquire different delay times (Fig. 32). Chirped gratings, therefore, can be used as dispersion compensators to compress temporally broadened pulses.

In telecommunication systems, residual pump light emitted from an optical fiber amplifier can cause major problems. The performance of a receiver can be adversely affected by the residual pump power emitted from a preamplifier because it can cause excess noise and receiver saturation. The fiber amplifier performance can be improved by reflecting back the unabsorbed pump light at the amplifier output.[81,82] Farries *et al.*[83] demonstrated the use of broadband chirped fiber Bragg grating for pump rejection and recycling of unabsorbed pump light from an erbium-doped fiber amplifier. In that work, an amplifier was pumped with a 980 nm diode laser and a broadband chirped fiber Bragg filter centered at 980 nm was used to reject and recycle the unabsorbed pump light. Fig. 33 shows the output spectrum of the emission from the amplifier, including the pump signal and amplified spontaneous emission, with and without the chirped grating filter attached to the doped fiber. Without the fiber filter [Fig. 33(a)], an unabsorbed pump power of 1 mW was measured, which was larger than the signal output power of 0.25 mW. With the fiber filter spliced to the output of the doped fiber [Fig. 33(b)], the residual pump power was reduced by 30 dB to 1 μW, the amplified spontaneous emission was decreased, and there was a small increase in the signal output power.

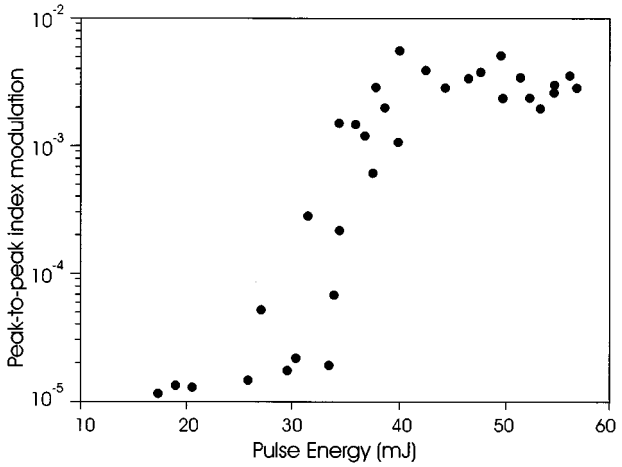

FIG. 34. Peak-to-peak modulation of induced refractive-index changes for different pulse energies (after Ref. 84).

4. Type II Bragg gratings

In an experiment carried out to study the relationship between pulse energy and grating strength, a series of single-pulse gratings were produced with an UV excimer laser beam.[84] The UV beam was focused to an area of approximately $15\times0.3\,\mathrm{mm}^2$ at the fiber. The peak-to-peak index modulation of each grating was estimated from its reflection spectrum using coupled-mode theory with the result summarized in Fig. 34. It is apparent that there is a sharp threshold at a pulse energy of 30 mJ, above which the induced index modulation increases dramatically. Doubling the pulse energy from 20 to 40 mJ results in an increase in the photoinduced index modulation by almost three orders of magnitude. Below the threshold point, the index modulation seems to grow linearly with energy density, whereas above the index modulation it appears to saturate. Figure 34 shows that these single-pulse Bragg gratings have induced index changes as high as 0.006, which is comparable to the core-cladding index difference of 0.02. The gratings formed with a low index of refraction modulation were labeled as *type I* and those formed with a high index of refraction modulation were called *type II*.

The behavior observed in Fig. 34 suggests that there is a critical level of absorbed energy, which triggers off a highly nonlinear mechanism, initiating dramatic changes in the optical fiber. Examination of a type II grating with an optical microscope revealed a damaged track at the core-cladding interface. This damage track appears only in type II gratings, which suggests that it may be responsible for the large index change. The fact that this damage is localized on one side of the core suggests that most of the UV light has been absorbed, most likely never reaching the other side. Although the origin of the process is not fully understood, Russell *et al.*[9] have proposed that the process is initiated by high single-photon absorption at 248 nm, exciting electrons into the conduction band of silica, where they seed the formation of a ''free''electron plasma. This would then produce an

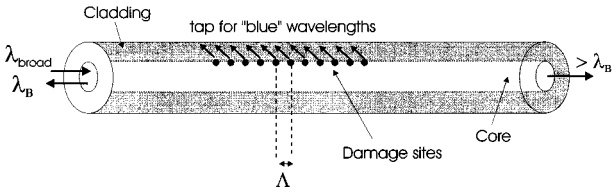

FIG. 35. Schematic diagram of a type II grating showing the damage track on one side of the fiber core. Wavelengths longer than the Bragg center wavelength are transmitted, whereas shorter wavelengths are strongly coupled into the cladding.

abrupt surge in UV absorption, and permanent damage in the glass. A schematic diagram of a type II grating is shown in Fig. 35.

A typical spectrum of a type II grating is shown in Fig. 36. A characteristic of type II Bragg gratings is that they have a very high reflectivity and large bandwidth. The irregularities in the spectra are a sign of grating nonuniformity, which is not surprising because of the nonuniformities in the intensity profile of the excimer laser writing beam. In addition, type II gratings transmit wavelengths longer than the Bragg center wavelengths but strongly couple shorter wavelengths into the cladding, permitting the gratings to act as effective wavelength selective taps.

Results of stability tests have shown type II gratings to be extremely stable at elevated temperatures. At 800 °C over a period of 24 h, no degradation in grating reflectivity was evident. At 900 °C, the grating reflectivity decays quite slowly until a permanent component appears. At 1000 °C, most of the grating disappears after 4 h. For comparison, as shown in Fig. 37, type I Bragg gratings are completely erased at 800 °C.[85] This provides evidence that the mechanism behind high-reflectivity type II single-pulse gratings differs from the usual type I mechanism. The superior temperature stability of type II gratings make them useful for sensing applications in hostile environments.

One of the most attractive features of type II gratings is that highly reflective gratings can be formed in just a few nanoseconds, the duration of a single excimer pulse. This is of great practical importance for large-scale mass production

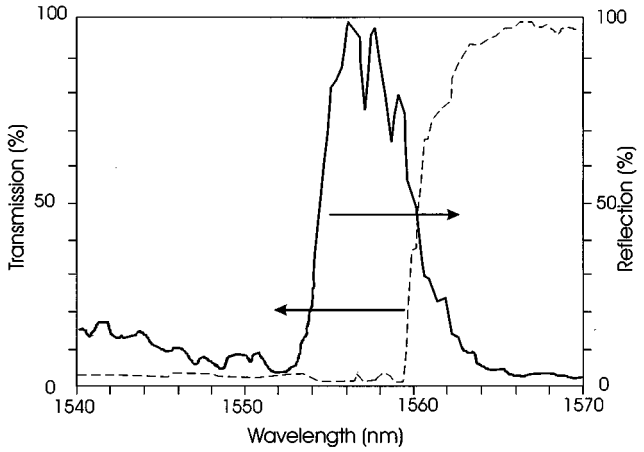

FIG. 36. Reflection and transmission spectra of a type II grating. For wavelengths below the Bragg wavelength (1556 nm), light is strongly coupled into the cladding (after Ref. 84).

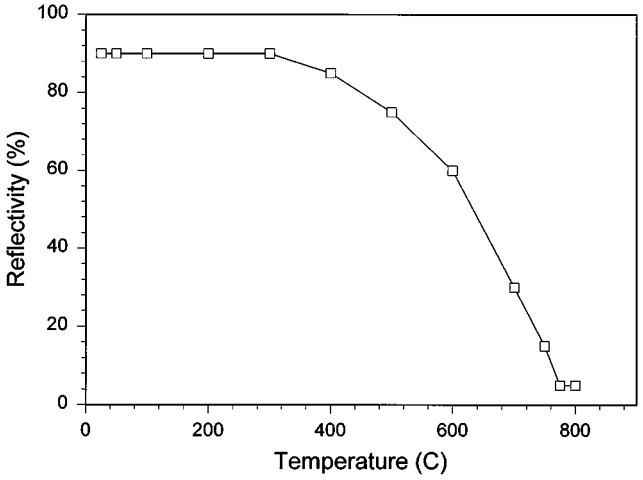

FIG. 37. Changes in reflectivity and center wavelength of a type I Bragg grating with temperature (after Ref. 85).

of strong gratings during the fiber drawing process before application of the protective polymer coating. Although the concept of fabrication of single-pulse type I and type II Bragg gratings during the fiber drawing process has been successfully demonstrated,[86,87] the quality of in-line gratings must be improved. One distinct advantage of producing fiber Bragg gratings during the draw process is that in-line fabrication avoids potential contact with the pristine outer surface of the glass. Whereas, off-line fabrication requires a section of the fiber to be stripped off its UV absorbing polymer coating, in order for the grating to be exposed. This drastically weakens the fiber at the site of the grating due to surface contamination, even if the fiber is subsequently recoated.

5. Novel Bragg grating structures

(a) *Superimposed multiple Bragg gratings.* Recently, the author and co-workers[88] demonstrated the inscription of several Bragg gratings at the same location on an optical fiber. This is of interest as a device in fiber communications, la-

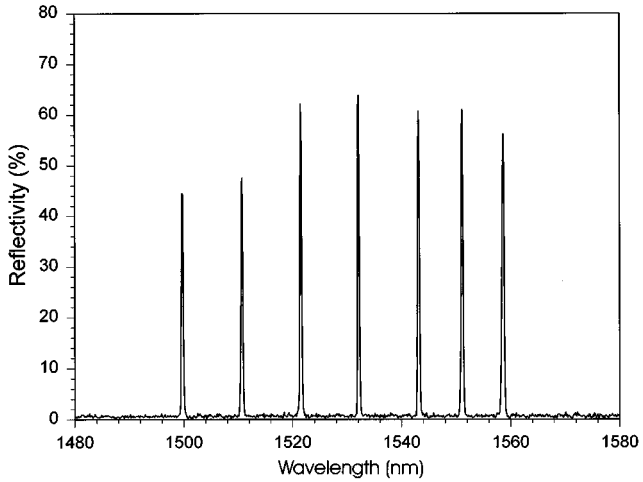

FIG. 38. Reflection spectrum for seven Bragg gratings superimposed at the same location on an optical fiber. The seven gratings cover a span of 60 nm ranging from 1500 to 1560 nm (after Ref. 88).

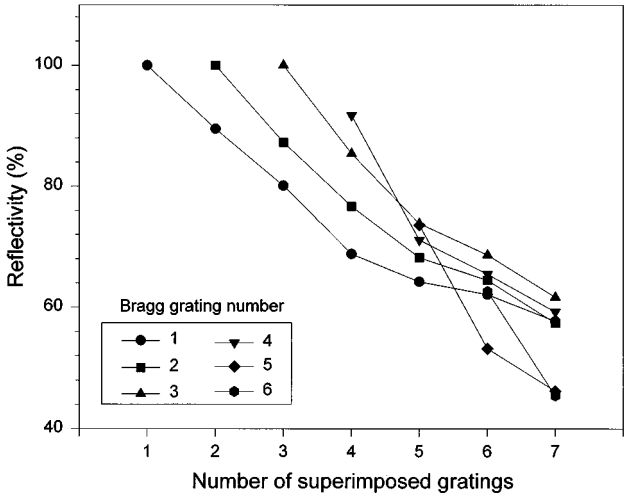

FIG. 39. Reflectivities for each Bragg grating as a function of the number of gratings superimposed on the same location. The lines through the symbols are a guide to the eye (after Ref. 88).

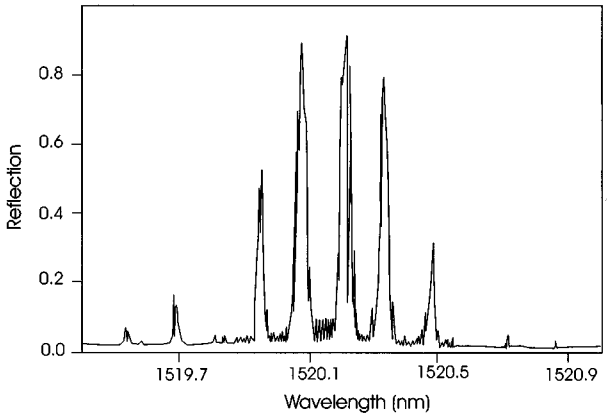

FIG. 40. Reflection spectrum from a grating superstructure fabricated by translating the UV writing beam along a fiber and phase-mask assembly while the intensity of the beam was modulated (after Ref. 89).

sers, and sensor systems. Because multiple Bragg gratings at the same location basically perform a comb function, this device is ideally suited for multiplexing and demultiplexing signals. The beauty of this device is that it does not require much space because all the gratings are written at the same location of the fiber. This lends itself to optical integrated technology, where the issue of size is always a concern, and can also be used for material detection where the multiple Bragg lines can be designed to match the signature frequencies of a given material. Figure 38 shows the reflectivity for seven Bragg gratings superimposed on the same area of the photosensitive fiber. Figure 39 illustrates a plot of the individual Bragg grating reflectivity as a function of the number of gratings written at the same location. Each time a new grating was inscribed, the reflectivity of the existing gratings was reduced. As shown (Fig. 39), even after superimposing five gratings, the reflectivity from each of the gratings was higher than 60%. Another interesting observation is that the center wavelength of the existing Bragg gratings shifted to longer wavelengths each time a new grating was inscribed due to a change of the effective index of refraction.

(b) *Superstructure Bragg gratings.* Superstructure Bragg grating is referred to a grating fiber structure fabricated with a modulated exposure over the length of the gratings.[89] One such approach used by Eggleton *et al.*[89] was to translate the UV writing beam along a fiber and phase-mask assembly while the intensity of the beam was modulated. They used an excimer pumped dye laser with a frequency doubler to produce 2.0 mJ at 240 nm. Hydrogenated, single-mode, boron-codoped fiber was placed in near contact with a phase mask, and the ultraviolet light was focused through the phase mask into the fiber core by a cylindrical lens, exposing a length of approximately 1 mm. To fabricate a 40 mm long superstructure, the excimer laser was periodically triggered at intervals of 15 s to produce bursts of 150 shots at a repetition rate of 10 Hz, while the ultraviolet beam was translated at a constant velocity of 0.19 mm/s along the mask. The resulting period of the grating envelope was approximately 5.65 mm, forming seven periods of the superstructure. The reflection spectrum of this grating structure is shown in Fig. 40. There is a strong reflection at five discrete wavelengths corresponding to the spatial frequencies of the grating, with reflectance varying from 30% to 95%. These superstructure gratings can be used as comb filters for signal processing, and for increasing the tunability of the fiber laser grating reflector.

(c) *Phase-shifted Bragg gratings.* Bragg gratings generally act as narrow-band reflection filters centered at the Bragg wavelength because of the stop band associated with a one-dimensional periodic medium. Many applications, such as channel selection in a multichannel communication system, would benefit if the fiber grating could be designed as a narrow-band transmission filter. Although techniques based on Michelson and Fabry–Perot interferometers have been developed for this purpose,[90] their use requires multiple gratings and may introduce additional losses. A technique commonly used in distributed feedback (DFB) semiconductor lasers[91,92] can be used to tailor the transmission spectrum to suit specific requirements. The technique consists of the introduction of phase shift across the fiber grating whose location and magnitude can be adjusted to design a specific transmission spectrum. It is a generalization of an idea first proposed by Haus and Shank[93] in 1976. The principle of the phase shift was demonstrated by Alferness *et al.*[94] in periodic structures made from semiconductor materials where a phase shift was introduced by etching a larger spacing at the center of the device. This forms the basis of single-mode phase-shifted semiconductor DFB lasers.[95] A similar device may be constructed in optical fibers using various techniques:

(1) Phase masks, in which phase-shift regions have been written into the mask design.[96]
(2) Postprocessing of a grating by exposure of the grating region to pulses of UV laser radiation, which has been described in Ref. 97 (Fig. 41).
(3) And postfabrication processing using localized heat treatment, which has also been reported.[98]

Such processing produces two gratings out of phase with each other, which act as a wavelength-selective Fabry–Perot resonator allowing light at the resonance to penetrate the stop

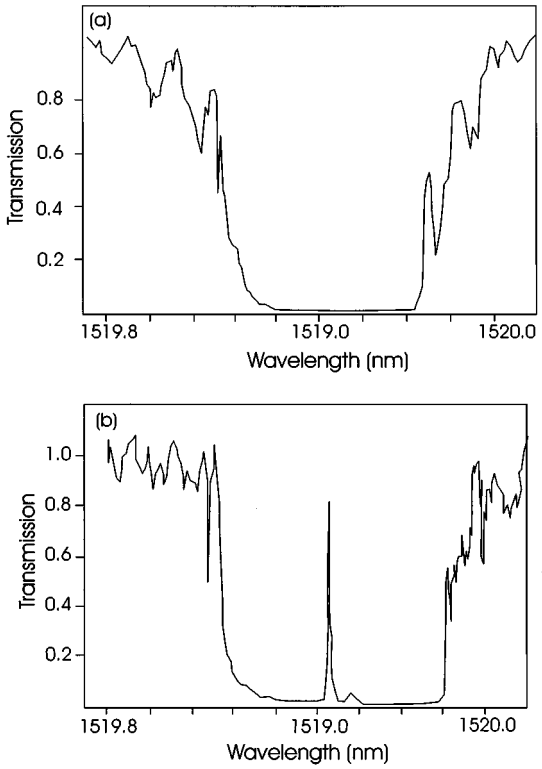

FIG. 41. Normalized transmission spectra before and after a phase shift induced in a Bragg grating structure using UV postprocessing (after Ref. 97).

band of the original grating. The resonance wavelength depends on the size of the phase change. One of the most obvious applications includes production of very narrow-band transmission and reflection filters. Moreover, multiple phase shifts can be introduced to produce other devices such comb filters. They can also be used to obtain single-mode operation of DFB fiber lasers.

V. SIMULATIONS OF SPECTRAL RESPONSE FROM BRAGG GRATINGS

A. *T*-matrix formalism

The spectral profile from a Bragg grating structure may be simulated using the *T*-matrix formalism. For this analysis, two counterpropagating plane waves are considered confined to the core of an optical fiber in which an intracore uniform Bragg grating of length l and uniform period Λ exist. This is illustrated in Fig. 42. The electric fields of the backward and forward waves can be expressed as $E_a(x,t)=A(x)\exp[i(\omega t-\beta x)]$ and $E_b(x,t)=B(x)\exp[i(\omega t+\beta x)]$, respectively, where β is the wave propagation constant. The complex amplitudes $A(x)$ and $B(x)$ of these electric fields obey the coupled-mode equations[99]

$$\frac{dA(x)}{dx}=i\kappa B(x)\exp[-i2(\Delta\beta)x], \qquad (0\leqslant x\leqslant l)$$
$$\frac{dB(x)}{dx}=-i\kappa^{*}A(x)\exp[i2(\Delta\beta)x], \tag{5.1}$$

where $\Delta\beta=\beta-\beta_0$ is the differential propagation constant (β_0 is π/Λ, and Λ is the grating period), and κ is the coupling coefficient. For uniform gratings, κ is constant and it is related to the index modulation depth. For a sinusoidal modulated refractive index, the coupling coefficient is real and it is given by $\pi\Delta n/\lambda$.

Assuming that there are both forward and backward inputs to the Bragg grating, and boundary conditions $B(0)=B_0$ and $A(l)=A_1$, then closed form solutions for $A(x)$ and $B(x)$ are obtained from Eq. (5.1). Following these assumptions, the closed form solutions for x dependencies of the two waves are $a(x)=A(x)\exp(-i\beta x)$ and $b(x)=B(x)\times\exp(i\beta x)$. Therefore, the backward output (reflected wave), a_0, and the forward output (transmitted wave), b_1, from the grating can be expressed by means of the scattering matrix[100]

$$\begin{bmatrix}a_0\\ b_1\end{bmatrix}=\begin{bmatrix}S_{11} & S_{12}\\ S_{21} & S_{22}\end{bmatrix}\cdot\begin{bmatrix}a_1\\ b_0\end{bmatrix}, \tag{5.2}$$

with $a_1=A_1\exp(i\beta l)$ and $b_0=B_0$, and

$$S_{11}=S_{22}=\frac{is\exp(-i\beta_0 l)}{-\Delta\beta\sinh(sl)+is\cosh(sl)},$$
$$S_{12}=S_{21}\exp(2i\beta_0 l)=\frac{\kappa\sinh(sl)}{-\Delta\beta\sinh(sl)+is\cosh(sl)}, \tag{5.3}$$

where $s=\sqrt{|\kappa|^2-\Delta\beta^2}$. Based on the scattering-matrix expression in Eq. (5.3), the T matrix for the Bragg is[101]

$$\begin{bmatrix}a_0\\ b_0\end{bmatrix}=\begin{bmatrix}T_{11} & T_{12}\\ T_{21} & T_{22}\end{bmatrix}\cdot\begin{bmatrix}a_1\\ b_1\end{bmatrix}, \tag{5.4}$$

where

$$T_{11}=T_{22}^{*}=\exp(-i\beta_0 l)\,\frac{\Delta\beta\sinh(sl)+is\cosh(sl)}{is},$$
$$T_{12}=T_{21}^{*}=\exp(-i\beta_0 l)\,\frac{\kappa\sinh(sl)}{is}. \tag{5.5}$$

The T matrix relates the input and output of the Bragg grating and is ideal for analyzing a cascade of gratings (Fig. 42). Figure 42(b) shows a series of gratings back to back with a total length L. This grating structure is made up of ''m'' Bragg grating segments. Each segment has a different period Λ_k and has its own T-matrix T, where $k=1,\ldots,m$.

The total grating structure may be expressed as

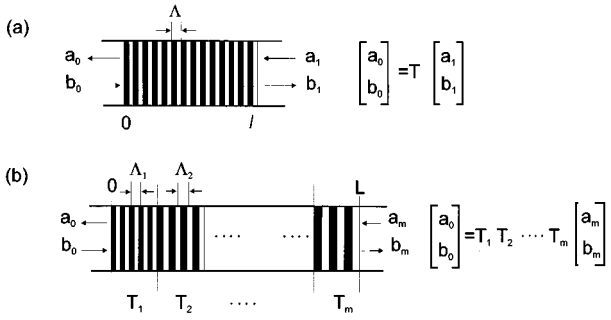

FIG. 42. Illustration of the *T*-matrix model: (a) a single uniform Bragg grating and (b) a series of gratings with different periods back to back.

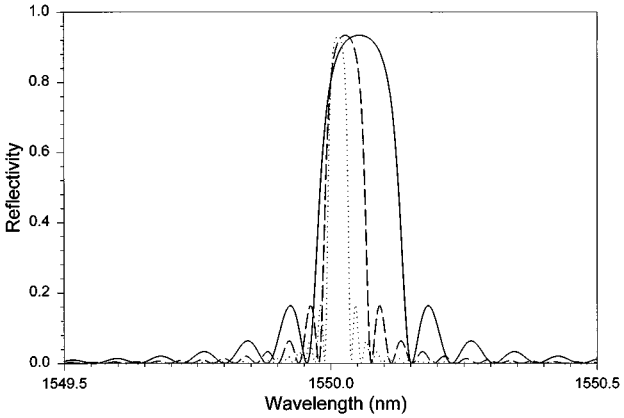

FIG. 43. Spectral profiles for uniform Bragg gratings. The various spectral profiles correspond to different grating lengths (1 cm; solid, 2 cm; dashed, and 4 cm; dotted).

$$\begin{bmatrix} a_0 \\ b_0 \end{bmatrix} = T_1 \cdot T_2 \cdots T_{m-1} \cdot T_m \cdot \begin{bmatrix} a_m \\ b_m \end{bmatrix}, \tag{5.6}$$

and the spectral reflectivity of the grating structure is given by $|a_0(\lambda)/b_0(\lambda)|^2$. It should be noted that this model does not take into account cladding-mode coupling losses. Next, the reflectivity spectral response of a few Bragg gratings structures will be calculated using this T-matrix formalism.

B. Uniform index of refraction Bragg gratings

1. Grating length dependence

The reflection spectral response for uniform Bragg gratings is calculated using the T-matrix formalism described above. The objective of this set of simulations is to demonstrate how the spectral response of a grating is affected as the length of the grating is altered. The index of refraction change is assumed uniform over the grating length, however, the value of the change is reduced accordingly with increasing grating length such that the maximum grating reflectivity remains constant. Figure 43 shows the spectral profile of three uniform Bragg gratings. Clearly, as seen from the various plots, the bandwidth of the gratings decreased with increasing length. The 1 cm long uniform grating had a bandwidth approximately of 0.15 nm, the 2 cm long grating was 0.074 nm and, finally, the 4 cm long grating was 0.057 nm. Theoretically, Bragg gratings may be constructed with extremely small bandwidths by simply increasing the grating length. However, in practice, such devices are not easy to manufacture. The error associated with the spacing between the periods of a grating (during manufacturing) is cumulative, therefore, with increasing grating length, the total error will increase, resulting in out-of-phase periods (leading to broadening of the Bragg grating). Furthermore, if a long perfect Bragg grating is constructed, the effects of the environment have to be considered very carefully. For example, any strain or temperature fluctuations on any part of the grating will cause the periods to move out of phase, resulting in broadening the spectral responses of the Bragg grating.

2. Index of refraction dependence

Figure 44 shows a set of simulations assuming a uniform

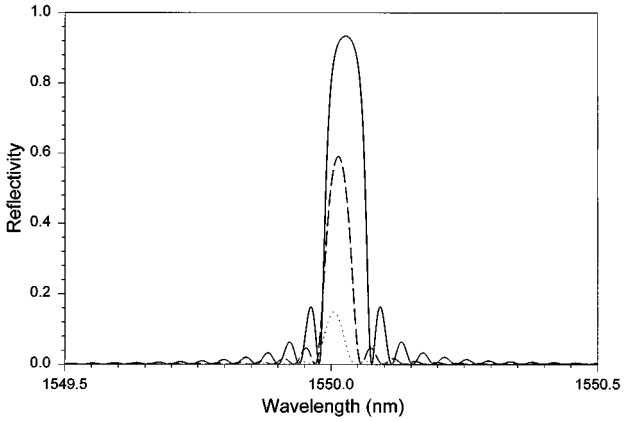

FIG. 44. Spectral reflectivity response from uniform Bragg grating 2 cm in length for different indexes of refraction. The solid line corresponds to 0.5×10^{-4} index of refraction change.

Bragg grating of 2 cm in length. In these simulations, the index of refraction changes were varied. For the first grating with $\Delta n = 0.5 \times 10^{-4}$, the reflectivity is 90% and the bandwidth is approximately 0.074 nm. Reducing the change of the index of refraction to half the value of the first grating ($\Delta n = 0.25 \times 10^{-4}$), the reflectivity decreases to 59% and the

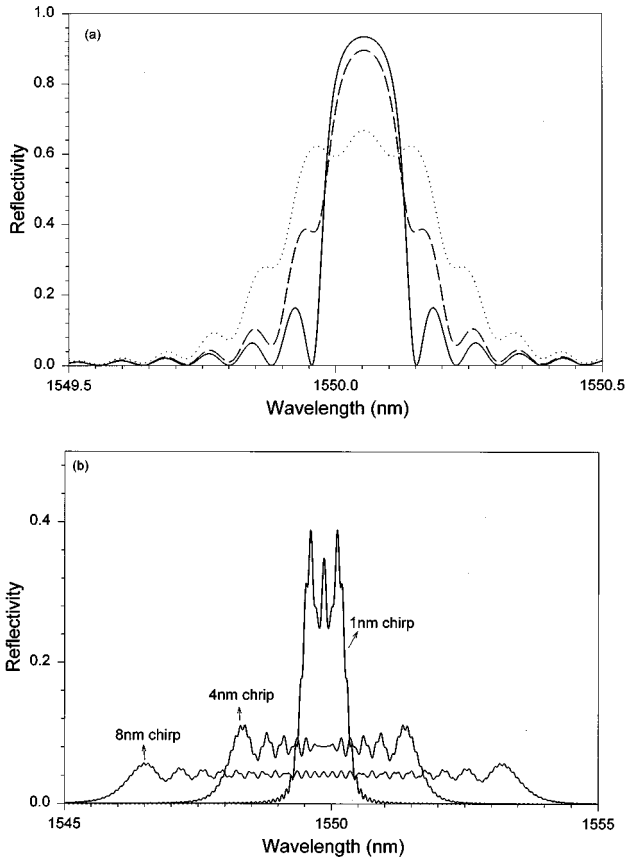

FIG. 45. (a) Spectral reflectivity response from different Bragg gratings showing the effect of chirping. All gratings are 10 mm and the index of refraction change is assumed 1×10^{-4} for all. The solid curve corresponds to 0 chirp, the dashed and dotted curves correspond to 0.2 and 0.4 nm chirp, respectively (where the chirp value is over the length of the grating). (b) Spectral reflectivity response from highly chirped Bragg gratings for the following chirp values of 1, 4, and 8 nm over the 10 mm length of the gratings.

bandwidth to 0.049 nm. A further decrease in the index of refraction change ($\Delta n = 0.1 \times 10^{-4}$) results in a reflectivity of 15% and a bandwidth of 0.039 nm. It appears that the bandwidth approaches a minimum value and remains constant for further reduction in the index of refraction change.

3. Chirped Bragg gratings

The simulations shown in Figs. 45(a) and 45(b) show chirped Bragg grating structures. Three different reflection spectra are shown in Fig. 45(a), corresponding to three different chirped values, 0, 0.2, and 0.4 nm over the entire length of the grating. In these simulations, all the gratings are assumed 10 mm in length with a constant index of refraction change 1×10^{-4}. With increasing chirp value, the reflectivity response becomes broader and the reflection maximum decreases. In these simulations, the chirp gratings are approximated with a number of progressively increasing period gratings whose total length amounts to the length of the chirp grating. The number of ''steps'' (the number of smaller gratings) assumed in the calculations are 100 (simulations indicated that calculations with more than 20 steps will give approximately the same result). Figure 45(b) shows the spectral response from Bragg gratings with very large chirp values (1, 4, and 8 nm over the 10 mm length of the grating). Clearly, with increasing chirp value, it is possible to span a very large spectral area, with a reduction in the maximum reflectivity of the grating. This problem may be overcome by increasing the index of refraction modulation.

C. Apodization of the spectral response of Bragg gratings

The reflection spectrum of a finite-length Bragg grating with uniform modulation of the index of refraction is accompanied by a series of sidelobes at adjacent wavelengths. It is very important to minimize and, if possible, eliminate the reflectivity of these sidelobes (or apodize the reflection spectrum of the grating) in devices where high rejection of the nonresonant light is required. An additional benefit of apodization is the improvement of the dispersion compensation characteristics of chirped Bragg gratings.[102] In practice, apodization is accomplished by varying the amplitude of the coupling coefficient along the length of the grating. A method used to apodize the response consists in exposing the optical fiber with the interference pattern formed by two nonuniform ultraviolet light beams.[103] In the phase-mask technique, apodization can also be achieved by varying the exposure time along the length of the grating, either from a double exposure or by scanning a small writing beam or using a variable diffraction efficiency phase mask. In all these apodization techniques, the variation in the coupling coefficient along the length of the grating comes from local changes in the intensity of the UV light reaching the fiber.

Figure 46 shows two plots of apodized grating with a Gaussian shape index of refraction change. The index of refraction changes are shown in the upper inset, which are plotted against the length of the grating. The full width at half-maximum of the index of refraction profile is doubled for one of the curves (the dotted curve), resulting in a larger

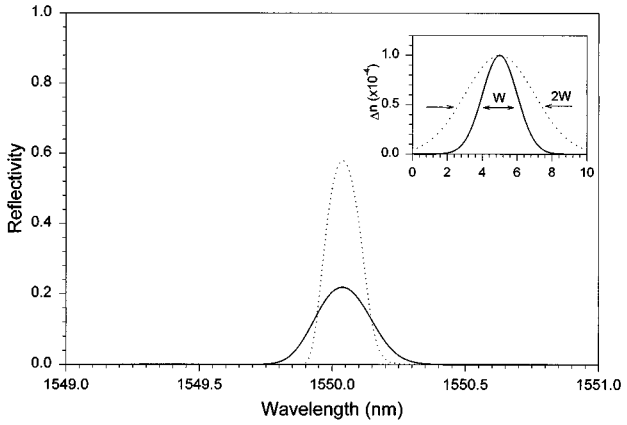

FIG. 46. Spectral reflectivity response from Gaussian apodised Bragg gratings. The apodization profiles plotted against the length of the gratings (10 mm) are shown in the inset at the upper-right corner.

spectral reflection response. It is interesting to point out that in both the apodized Bragg gratings the sidelobes have been eliminated.

Apodization of the spectra response of fiber Bragg gratings using a phase mask with variable diffraction efficiency has been reported by Albert *et al.*[104] Bragg gratings with sidelobe levels 26 dB lower than the peak reflectivity have been fabricated in standard telecommunication fibers. This represents a reduction of 14 dB in the sidelobe levels compared to uniform gratings with the same bandwidth and reflectivity. Figure 47 shows the spectral reflection response of an apodized and an unapodized fiber Bragg grating reflector reported by the same group,[105] where they have achieved a reduction of 20 dB in the sidelobe levels.

A cosine apodization technique has been reported recently by Kashyap *et al.*[106] obtained by repetitive, symmetric longitudinal stretching of the fiber around the center of the grating while the grating was written. This apodization scheme is applicable to all types of fiber gratings, written by direct replication by a scanning or a static beam, or by use of any other interferometer, and is independent of length. The simplicity of this technique allows the rapid production of fiber gratings required for wavelength-division multiplexed systems (WDM) and dispersion compensation.

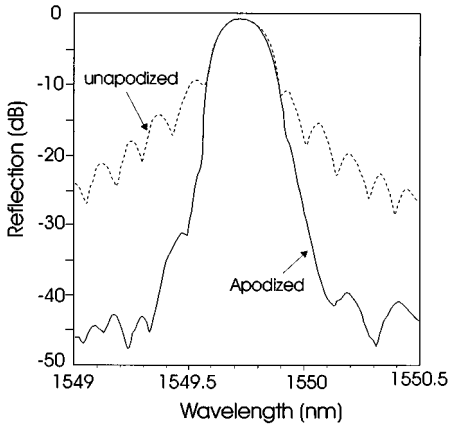

FIG. 47. Reflection spectrum of fiber Bragg gratings photoimprinted with a uniform diffracting phase mask and with a phase mask with a Gaussian profile of diffraction efficiency (after Ref. 105).

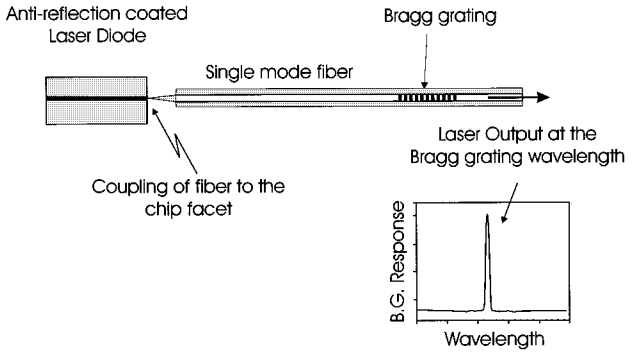

FIG. 48. External fiber grating semiconductor laser. The semiconductor laser chip is antireflection coated on the output face and coupled to a fiber with a Bragg grating, forcing oscillation at the Bragg grating wavelength.

VI. APPLICATIONS OF BRAGG GRATINGS

A. Fiber Bragg grating diode laser

A fiber Bragg grating may be coupled to a semiconductor laser chip to obtain a fiber Bragg diode laser.[107] A semiconductor laser chip is antireflection coated on the output facet and coupled to a fiber with a Bragg grating as illustrated in Fig. 48. If this Bragg grating reflects at the gain bandwidth of the semiconductor material, it is possible to obtain lasing at the Bragg grating wavelength. The grating bandwidth can be narrow enough to force single-frequency operation with a linewidth of much less than a gigahertz. High output powers, up to 20 mW, have been obtained with these types of lasers.[108] An added advantage of these systems is that the grating has a temperature sensitivity around 10% of that of the semiconductor laser, reducing temperature induced wavelength drift. These fiber grating semiconductor laser sources have been used to generate ultrashort mode-locked soliton pulses up to 2.9 GHz.[109]

One problem in distributed Bragg reflector (DBR) laser manufacture is the precise control of the laser wavelength. Routine production of DBR lasers with a wavelength specified to better than 1 nm is difficult, but optical Bragg gratings can be manufactured precisely to the wavelength required. With antireflection coating on the semiconductor chip, the lasing wavelength may be selected from anywhere in the gain bandwidth by choosing the appropriate fiber Bragg grating. Clearly, such an approach will increase the yield from the semiconductor wafers. In addition, since each laser has to be coupled to a fiber, the Bragg grating may be written after the packaging process has proved to be successful, thus, reducing the time spent on unsuccessful products.

B. Fiber Bragg grating lasers

The majority of Bragg grating fiber laser research has been on erbium-doped lasers due to its potential in communication and sensor applications. The characteristic broadband gain profile of the erbium-doped fiber around the 1550 nm region makes it an extremely useful tunable light source. Employing this doped fiber in an optical cavity as the lasing medium, along with some tuning element, results in a continuously tunable laser source over its broad gain profile. In fact, a tunable erbium-doped fiber with an external grating

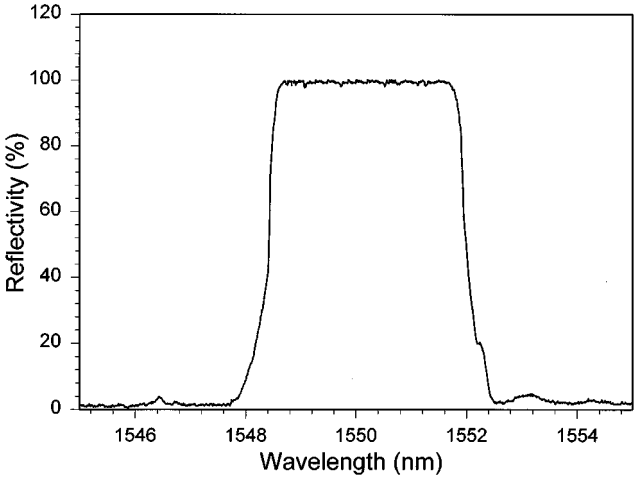

FIG. 49. Measured reflection spectra from the long grating mirror written in a photosensitive telecommunication fiber using a KrF excimer laser in an interferometric setup (after Ref. 117).

was reported by Reekie *et al.*[110] in 1986. Since then, several laser configurations have been demonstrated with two or more intracavity gratings.[111–116]

A simple Bragg grating tunable Er-doped fiber laser was demonstrated by the author and co-workers, where a broadband Bragg mirror and a narrow Bragg grating served as the high reflector and the output coupler, respectively.[117] The broadband Bragg mirror was constructed by writing five Bragg gratings, each separated spectrally by approximately 0.5 nm. The resultant spectral profile of this Bragg mirror is shown in Fig. 49. The fiber laser consisted of a 2 m long erbium-doped fiber with Bragg gratings at each end (broadband and narrow band) providing feedback to the laser cavity. The output coupler to the fiber laser cavity was a single grating with approximately 80% reflectivity and 0.12 nm linewidth. Figure 50 shows the broadband fluorescence obtained from the Er-doped fiber laser system before the lasing threshold is reached. The spectrum is the typical characteristic broadband gain profile from an erbium-doped fiber spanning a range of several tens of manometers, namely, between 1.45 and 1.65 μm. Superimposed on the gain profile is a

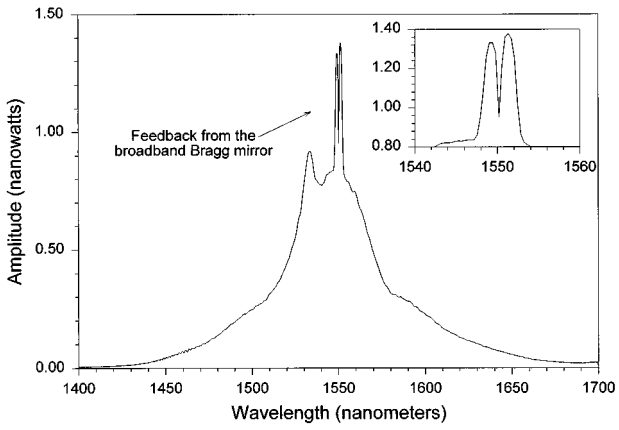

FIG. 50. Broadband fluorescence obtained from an erbium-doped fiber laser. Superimposed on the gain profile is the broadband mirror at 1550 nm. Within this peak there is a notch at 1550 nm corresponding to the Bragg grating (after Ref. 117).

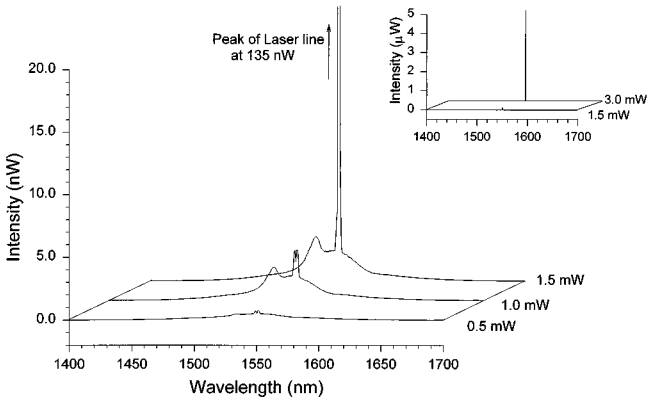

FIG. 51. Output spectrum from erbium-doped fiber laser at various coupled input powers varying from below the lasing threshold of 0.5 mW to nearly lasing at 1.0 mW and fully lasing at 1.5 mW. The inset at the upper-left corner shows the lasing spectrum as a function of coupled pump power of 1.5 and 3.0 mW (note that the laser power at 3 mW is approximately 40 times stronger than that at 1 mW).

broadband peak (3.5 nm) at 1550 nm corresponding to the reflection of the fluorescence from the broadband Bragg mirror, and within this peak there is a notch at 1550 nm corresponding to the narrow Bragg grating. With increasing incident pump power, the losses in the fiber laser cavity are overcome and lasing begins. At pump powers just above threshold value, the notch due to the Bragg grating begins to grow in the positive direction and as the pump power increases further, the laser grows even stronger by depleting the broadband fluorescence (Fig. 51). In Fig. 51, the output spectrum, from the erbium-doped fiber laser, is shown for various coupled pump powers into the doped fiber, starting below the lasing threshold at 0.50–1.0 mW and 1.5 mW, where the laser line at 1550 nm begins to grow. At 3.0 mW of the coupled pump power, lasing is dominant. This is shown in the inset at the upper left-hand corner where a vertical line at 1550 nm represents the lasing wavelength.

Single-frequency Er^{3+}-doped Fabry–Perot fiber lasers using fiber Bragg gratings as the end mirrors[67,118] are emerging as an interesting alternative to DFB diode lasers for use in future optical CATV networks and high capacity WDM communication systems.[119] They are fiber compatible, simple, scaleable to high output powers, and have a low noise and kilohertz linewidth. In addition, the lasing wavelength can be determined to an accuracy of better than 0.1 nm, which is very difficult to achieve with DFB diode lasers.

Fiber lasers can operate in a single-frequency mode, provided that the grating bandwidth is kept below the separation between the axial mode spacings. Furthermore, it is necessary to keep the erbium concentration low enough (a few 100 ppm) to reduce ion-pair quenching, which causes a reduction in the quantum efficiency, and in addition may lead to strong self-pulsation of the laser.[118–120] The combination of these practical limits implies that the pump absorption of an erbium-doped fiber system can be as low as a few percent, resulting in low output lasing power. One solution to this problem is to use the residual pump power to pump an erbium-doped fiber amplifier following the fiber laser.[121] However, in such cases the amplified spontaneous emission

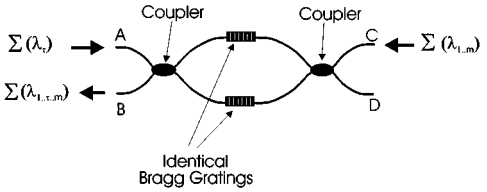

FIG. 52. Schematic diagram of a drop–add filter formed by adding a second coupler to close the legs containing the grating of a Mach–Zehnder arrangement.

from the amplifier increases the output noise. Another way to overcome the problem of low pump absorption is by codoping the erbium-doped fiber with Yb^{3+}.[122] This increases the absorption at the pump wavelength by more than two orders of magnitude and enables high efficient operation of centimeter long lasers with relatively low Er^{3+} concentration. Kringlebotn *et al.*[123] reported a highly efficient, short, robust single-frequency and linearly polarized Er^{3+}:Yb^{3+}-codoped fiber laser with fiber grating Bragg reflectors, an output power of 19 mW, and a linewidth of 300 kHz for 100 mW of 980 nm diode pump power.

Rare-earth-doped fiber lasers emitting at around 2 μm have potential uses in medical application, eye-safe LIDAR, and sensors. Continuous lasers in the 2 μm band using doped fiber has been reported since 1988.[124–127] All these lasers involved silica or fluoride based fibers codoped with thulium and/or holmium. Boj *et al.*[128] have demonstrated a diode pumped thulium-doped silica fiber laser with intracore Bragg gratings in the 1.9–2.1 μm band.

C. Filters and mode converters

A single Bragg grating in a single-mode fiber acts as a wavelength-selective distributed reflector or a band rejection filter by reflecting wavelengths around the Bragg resonance. However, by placing identical gratings in two lengths of a fiber coupler, as in a Michelson arrangement, one can make a bandpass filter.[129] This filter, shown in Fig. 28(a), passes only wavelengths in a band around the Bragg resonance and discards other wavelengths without reflections. If the input port is excited by broadband light and the wavelengths reflected by the gratings arrive at the coupler with identical optical delays, then this wavelength simply returns to the input port. If, however, a path-length difference of $\pi/2$ is introduced between the two arms, then it is possible to steer the reflected wavelength to arrive at the second input port, creating a bandpass filter. In principle, this is a low-loss filter, however, there is a 3 dB loss penalty for the wavelengths that are not reflected, unless a Mach–Zehnder interferometer is used to recombine the signal at the output.[130] An efficient bandpass filter was demonstrated by Bilodeau *et al.*[131,132] using a scheme identical to that presented in Ref. 130. The device had back reflection of -30 dB. However, all wavelengths out of the pass band suffered from the 3 dB loss associated with the Michelson interferometer.

Optical fiber communication systems employing wavelength division multiplexing/demultiplexing (WDM/D) techniques require low-loss, compact, stable, and reliable components, which can be used as wavelength-selective channel

dropping or inserting filters. By adding a second coupler to close the legs containing the gratings of Fig. 28(a), as in a Mach–Zehnder arrangement, one can make a drop–add filter[133] (Fig. 52). The Mach–Zehnder is balanced so that any optical signal in the 1550 nm transmission window launched into the input fiber (port A or C) is coupled into the output fiber (port D or B). The two identical Bragg reflection filters and the input coupler, which has a precise 50:50 splitting ratio at the center wavelength of the reflection gratings, form a Michelson interferometer transmission filter. The path length in each arm of the interferometer is set equal, thus, giving maximum transmission. Any signal launched into port A, at the transmission wavelength of the Michelson interferometer, will be coupled into port B. An input optical signal $\Sigma(\lambda_\tau)$, at the transmission wavelength of the Michelson interferometer (λ_τ), can be multiplexed onto an optical signal containing many discrete wavelengths $\Sigma(\lambda_{1\cdots m})$ by launching into ports A and C, respectively, with the output signal $\Sigma(\lambda_{1\cdots\tau\cdots m})$ being transmitted into port B. Conversely, an optical signal $\Sigma(\lambda_\tau)$ can be demultiplexed into port B from an optical signal containing many discrete wavelengths $\Sigma(\lambda_{1\cdots\tau\cdots m})$ launched into port A, with the remainder of the signal $\Sigma(\lambda_{1\cdots m})$ being transmitted into port D.

Placing two identical Bragg gratings in series on a single-mode fiber results in a Fabry–Perot etalon within the fiber core. Figure 28(b) shows one such construction with 99.5% reflectors, a free-spectral range of 1.06 GHz, and a finesse of 660. With the advancements in the inscription of Bragg gratings in optical fiber, it is now possible to obtain etalons with finesse, as high as several thousands.

By tilting or blazing the Bragg grating at angles to the fiber axis, light can be coupled out of the fiber core into loosely cladding modes or to radiation modes outside the fiber.[74] This wavelength-selective tap occurs over a rather broad range of wavelengths that can be controlled by the grating and waveguide design. One of the advantages is that the signals are not reflected in, thus, the tap forms an absorption-type filter. An application, that was already mentioned in Sec. IV B 2 is that this grating tap can be used as a gain flattening filter for an erbium fiber amplifier.

With a small tilt of the grating planes to the fiber axis ($\sim 1°$), one can make a reflecting spatial-mode coupler such that the grating reflects one guided mode into another. It is interesting to point out that by making long-period gratings, one can perturb the fiber to couple to other forward going modes. A wavelength filter based on this effect has been demonstrated by Hill *et al.*[58] The spatial-mode converting grating was written using the point-by-point technique with a period of 590 μm over a length of 60 cm. Using mode strippers before and after the grating makes a wavelength filter. In a similar manner, a polarization-mode converter or rocking filter in polarization maintaining fiber can be made. A rocking filter of this type, generated with the point-by-point technique, was demonstrated by Hill and co-workers.[59] In their work, they demonstrated an 87 cm long, 85 step rocking filter, which had a bandwidth of 7.6 nm and a peak transmission of 89%.

D. Pulse dispersion compensation

One of the main problems that occur in single-mode optical fibers is chromatic dispersion, causing different wavelength components of a data pulse to travel at different group velocities. This causes broadening of the signal pulse and increasing bit-error rates. With increasing network data rates, chromatic dispersion in standard single-mode fiber is the main limiting factor in performance. For a low data rate of 2.5 Gbit/s, a signal can be transmitted without significant degradation for up to 1000 km. However, this distance drops to 60 km at 10 Gbit/s and to 15 km at 20 Gbit/s. In addition, a large portion of the already worldwide installed fiber is optimized for transmission at 1.31 μm. This type of fiber exhibits high chromatic dispersion of the order of 17 ps/nm km when used to transmit at the more commonly used telecommunication wavelength of 1.55 μm.

Chirped fiber Bragg gratings provide the means for dispersion compensation. The basic principle of operation of a chirped fiber grating as a dispersion compensating element is that different wavelength components of the broadened pulse are reflected from different locations along the Bragg grating. Therefore, the dispersion imparted by the grating in reflection to a pulse with a given spectral content is equal to twice the propagation delay through the grating length L as

$$\tau = \frac{2L}{v_g}, \tag{6.1}$$

where v_g is the group velocity of the pulse incident on the grating. Therefore, a grating with a linear wavelength chirp of $\Delta\lambda$ nm will have a dispersion of

$$d = \frac{\tau}{\Delta\lambda}\ (\text{ps/nm}). \tag{6.2}$$

Eggleton *et al.*[46] demonstrated dispersion compensation by pulse compression with the use of a chirped grating. Figures 53(a) and 53(b) show, respectively, the 21 ps input pulse and the compressed 13 ps reflected pulse. To show that the observed compression is not due to truncation of the pulse spectrum by the grating, the direction of the grating was reversed, which resulted in the pulse stretching to 40 ps as shown in Fig. 53(c). Pulse stretching is expected because the sign of the dispersion in the reversed case adds to the dispersion of the optical pulse.

Fiber dispersion compensation using a chirped fiber Bragg grating was demonstrated by Williams *et al.*[134] They used short pulses (Fig. 54) and gave an experimental demonstration of the use of a chirped Bragg grating to compensate for the pulse broadening arising from negative group delay dispersion and nonlinear self-phase modulation in a length of fiber. Short pulses of 1.8 ps were sent through 200 m of optical fiber, which had a measured group delay dispersion of -100 ps/nm km. These pulses suffered significant dispersive broadening in the fiber. A 50:50 coupler between the fiber and a linearly chirped fiber Bragg grating provided output of the pulses directly from the fiber and those reflected off the grating. These pulses were measured temporally by cross correlating them with pulses taken directly from the laser.

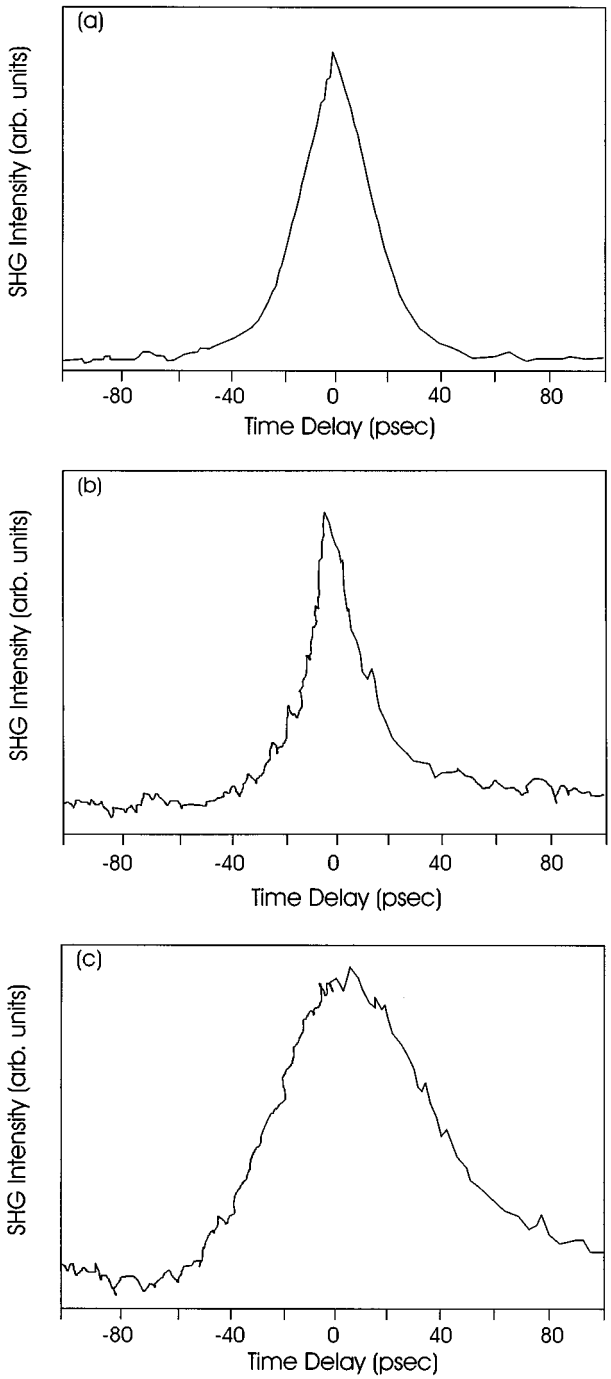

FIG. 53. Traces of optical pulses before and after reflection from a chirped grating. (a) The initial chirped pulse with duration of 21 ± 1 ps, (b) compressed pulse after reflection from a chirped grating with duration of 13 ± 1 ps, and (c) stretched pulse after reflection from a reversed chirped grating with duration of 40 ± 1 ps. From Eggleton *et al.* (after Ref. 46).

E. Fiber Bragg gratings sensors

Fiber Bragg gratings are excellent fiber-optic sensing elements. They are integrated into the light guiding core of the fiber and are wavelength encoded, eliminating the problems of amplitude or intensity variations that plague many other types of fiber sensors. Due to their narrow-band wavelength reflection, they are also conveniently multiplexed in a fiber-optic network. Fiber gratings have been embedded in composite materials for smart structures monitoring, and tested with civil structures to monitor load levels. They have also been successfully tested as acoustic sensing arrays. Applications for fiber grating sensors should also be emerging in process control and aerospace industries in the near future.

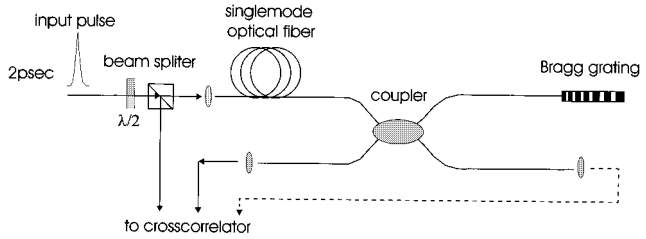

FIG. 54. Experimental configuration used to investigate dispersion compensation of a linearly chirped fiber Bragg grating.

The temperature sensitivity of a Bragg grating occurs principally through the effect on the index of refraction and to a lesser extent through the expansion coefficient (*this is described in detail in Sec. IV B 3*). It is noteworthy that temperature sensitivity can be enhanced or mulled by proper bonding to other materials. The maximum operating temperatures may be around 500 °C, however, this may depend on the fabrication condition of the Bragg grating. For example, type II gratings may operate at higher temperatures than type I gratings.

Strain affects the Bragg response directly through the expansion or contraction of the grating elements and through the strain-optic effect (see Sec. IV B 3). Many other physical parameters other than tension can also be measured such as pressure, flow, vibration acoustics, acceleration, electric, magnetic fields, and certain chemical effects. Therefore, fiber Bragg gratings can be thought off as generic transducer elements. There are various schemes for detecting the Bragg resonance shift, which can be very sensitive. One such scheme involves the injection of a broadband light (generated by a super-luminescent diode, edge-emitting light-emitting diode, erbium-doped fiber super-fluorescent source) into the fiber and determining the peak wavelength of the reflected light. Another way involves the interrogation of the Bragg grating with a laser tuned to the sensor wavelength, or by using the sensor as a tuning element in a laser cavity. Detecting small shifts in the Bragg wavelength of fiber Bragg grating sensor elements, which corresponds to changes of the sensing parameter is important. In a laboratory environment, this can be accomplished using a high-precision optical spectrum analyzer. In practical applications, this function must be performed using compact, low-cost instrumentation. Schemes based on simple broadband optical filtering, interferometric approaches, and fiber laser approaches allow varying degrees of resolution and dynamic range, and should be suitable for most applications.

The most straightforward means for interrogating a Bragg grating sensor is based on a passive broadband illumination of the device. Light with a broadband spectrum, which covers that of the Bragg grating sensor, is input to the system, and the narrow-band component reflected by the grating is directed to a wavelength-detection system. Several options exist for measuring the wavelength of the optical signal reflected from a Bragg grating element including a

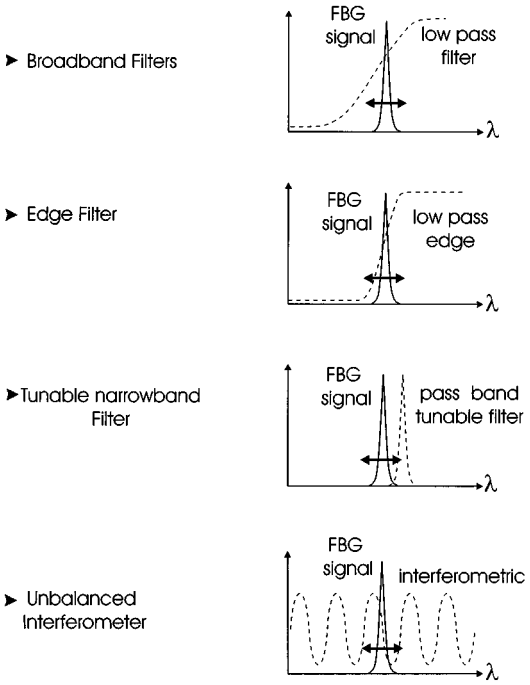

FIG. 55. Diagram of basic filtering function for processing fiber Bragg grating return signals.

miniaturized spectrometer, passive optical filtering, tracking using a tunable filter, and interferometric detection. The optical characteristics of these filtering options are as shown in Fig. 55. Filtering techniques based on the use of broadband filters allow the shift in the Bragg grating wavelength of the sensor element to be assessed by comparing the transmittance through the filter compared to a direct ''reference'' path.[135] A relatively limited sensitivity is obtained using this approach due to problems associated with the use of bulk-optic components and alignment stability. One way to improve this sensitivity is to use a fiber device with a wavelength-dependent transfer function, such as a fiber WDM coupler. Fused WDM couplers for 1550/1570 nm operation are commercially available. This coupler will provide a monotonic change in the coupling ratio between two output filters for an input optical signal over the entire optical spectrum of an erbium broadband source, and thus, has a suitable transfer function for wavelength discrimination over this bandwidth. An alternate means to increasing the sensitivity is to use a filter with a steeper cutoff [see Fig. 55(b)], such as an edge filter. However, this can limit the dynamic range of the system. One of the most attractive filter based techniques for interrogating Bragg grating sensors is based on the use of a tunable passband filter for tracking the Bragg grating signal. Examples of these types of filters include Fabry–Perot filters,[136] acousto-optic filters,[137,138] and fiber Bragg grating based filters.[139]

1. Tunable filter interrogation

Figure 56 shows the configuration used to implement a tunable filter (such as a fiber Fabry–Perot) to interrogate a Bragg grating sensor. The fiber Fabry–Perot can be operated in either a tracking or scanning mode for addressing single or multiple grating elements, respectively. In a single sensor

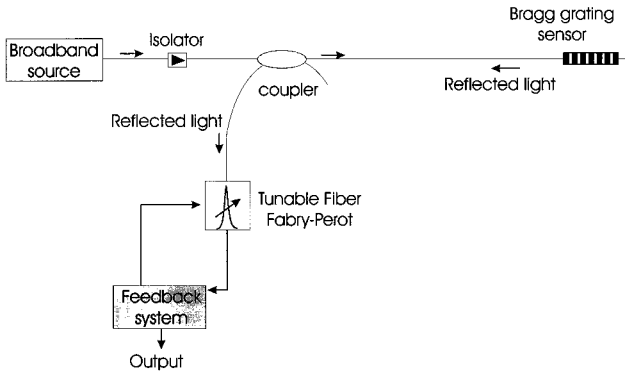

FIG. 56. Schematic of a tuned filter based interrogation technique for fiber Bragg grating sensor.

configuration, the Fabry–Perot filter with a bandwidth of 0.1 nm is locked to the Bragg grating reflected light (R) using a feedback loop. This is accomplished by dithering the fiber Fabry–Perot resonance wavelength by a small amount (typically, 0.01 nm) and using a feedback loop to lock to the Bragg wavelength of the sensor return signal. The fiber Fabry–Perot control voltage is a measure of the mechanical or thermal perturbation of the Bragg grating sensor.

Operating the fiber Fabry–Perot filter in a wavelength-scanning mode provides a means for addressing a number of fiber Bragg gratings elements placed along a fiber path (Fig. 57). In this mode, the direct Bragg grating sensor spectral returns are obtained from the photodetector output. The minimum resolvable Bragg wavelength shift that can be detected has limited resolution. By dithering the Fabry–Perot filter transmission, the derivative response to the spectral components in the array output can be obtained, producing a zero crossing at each of the Bragg grating center wavelengths, and thus, improving the resolution in determining the wavelength shifts, and hence, the strain (or any other sensing parameter for which the transducer is made).

2. Interferometric interrogation

A sensitive technique for detecting the wavelength shifts of a fiber Bragg grating sensor makes use of a fiber interferometer. The principle behind such a system is shown in Fig. 58. Light from a broadband source is coupled along a fiber to the Bragg grating element. The wavelength component re-

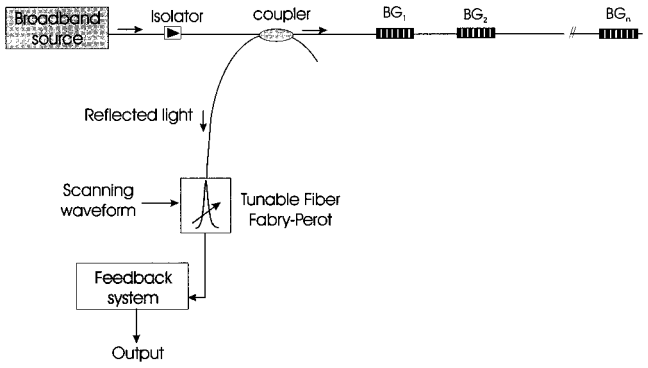

FIG. 57. Schematic of a multiplexed fiber Bragg grating sensor array with a scanning Fabry–Perot filter.

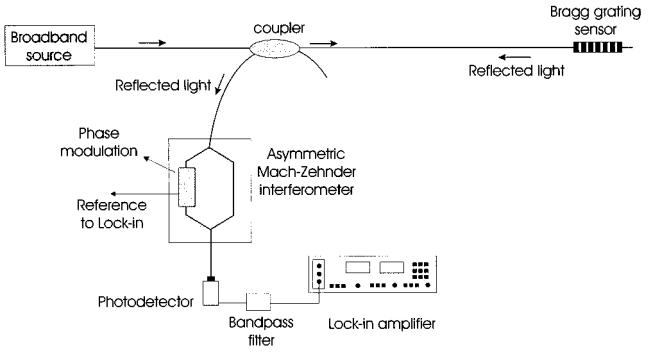

FIG. 58. Schematic of an interferometer interrogation technique for a fiber Bragg grating sensor.

flected back along the fiber toward the source is tapped off and fed to unbalance Mach–Zehnder interferometer. This light, in effect, becomes the light source into the interferometer, and the wavelength shifts induced by perturbation of the Bragg grating sensor resemble a wavelength modulated source. The unbalanced interferometer behaves as a spectral filter with a raised cosine transfer function. The wavelength dependence on the interferometer output can be expressed as

$$I(\lambda_b)=A\left[1+k\,\cos\left(\frac{2\pi nd}{\lambda_b}+\phi\right)\right], \tag{6.3}$$

where A is proportional to the input intensity and system losses, d is the length imbalance between the fiber arms, n is the effective index of the core, λ_b is the wavelength of the return light from the grating sensor, and ϕ is a bias phase offset of the Mach–Zehnder interferometer. Pseudoheterodyne phase modulation is used to generate two quadrature signals with a 90° phase shift with respect to each other, thus, providing directional information. Wavelength shifts are tracked using a phase demodulation system developed for interferometric fiber-optic sensors. In practical applications, a reference wavelength source is used to provide low-frequency drift compensation. Strain resolution as low as $0.6n\epsilon/\mathrm{Hz}^{-0.5}$ at 500 Hz have been reported.[140]

A combination of a wavelength filter and fiber interferometer to increase the number of gratings interrogated, while maintaining the high resolution offered by the phase sensitive detection scheme, has also been realized.[141]

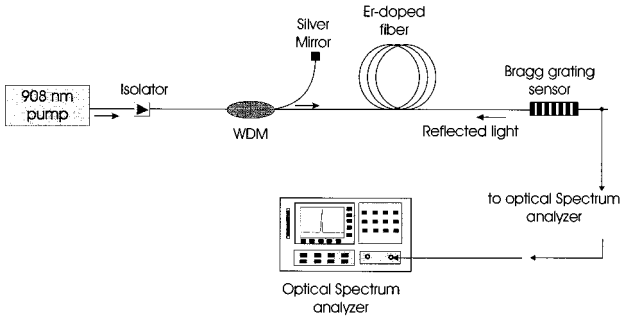

FIG. 59. Schematic of a fiber laser sensor configuration with fiber Bragg grating elements.

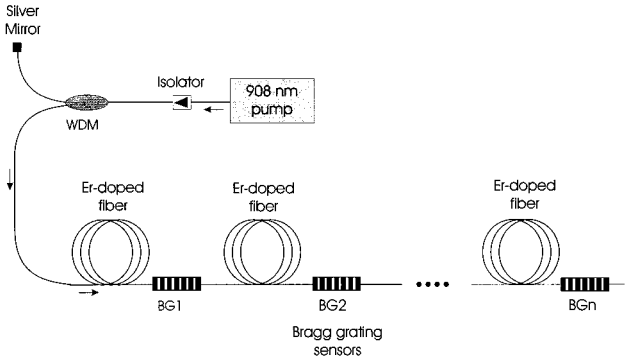

FIG. 60. Schematic configuration of a serially m multiplexed Bragg grating fiber laser.

3. Active laser interrogation

In active interrogation, the fiber Bragg grating sensor is used as an optical feedback element of an optical laser cavity.[71] Compared to the passive broadband base system, forming a fiber Bragg laser sensor generally provides stronger optical signals, and thus, has the potential to provide improved signal-to-noise performance. The basic concept is shown in Fig. 59. The laser cavity is formed between the mirror and the fiber Bragg grating element, which may be located at some sensing point. A gain section within the cavity can be provided via a semiconductor or doped fiber (such as the erbium-doped fiber). Once the laser gain is greater than unity, the fiber laser will lase at the wavelength determined by the fiber Bragg grating wavelength. As the Bragg grating changes its periodicity due to strain or temperature, the lasing wavelength will also shift. Reading of the laser wavelength using filtering, tracking filters, or interferometric techniques can then be used to determine induced shifts. This laser sensor configuration, however, is limited to a single fiber Bragg grating element. A means to increase the number of Bragg gratings that can be addressed is to incorporate an additional tuning element within the cavity, which selectively optimizes the gain at certain wavelengths. In this way, a number of fiber Bragg gratings, each operating at nominally different wavelengths, can be addressed in a sequential manner to form a quasidistributed fiber laser sensor. By tuning a wavelength selective filter located within the laser cavity over the gain bandwidth, the laser selectively lases at each of the Bragg wavelengths of the sensors. Thus, strain induced shifts in the Bragg wavelengths of the sensors are detected by the shift in the lasing wavelengths of the system.

An alternative multiplexed fiber laser sensor is based on a single element fiber laser sensor utilizing a WDM (see Ref. 73). Theoretically, since erbium is a homogeneously broadened medium, it will support only one lasing line simultaneously. To produce several laser lines within a single length of optical fiber, a section of erbium-doped fiber is placed between the successive Bragg gratings. With sufficient pump power and enough separation between the Bragg grating center wavelengths, a multiplexed fiber lasers sensor is possible. The maximum number of sensors utilized would depend on the total pump power, the required dynamic range, and finally, the gain profile of the active medium. A schematic configuration of the serially multiplexed Bragg grating fiber

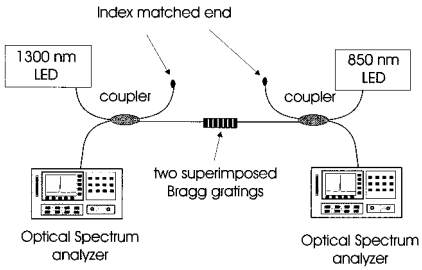

FIG. 61. Schematic diagram for measuring simultaneously strain and temperature using two superimposed Bragg gratings at 1300 and 850 nm.

laser is shown in Fig. 60. One of the drawbacks in such a serial multiplexed configuration is that the cavities are coupled so their respective gains are not independent. In fact, gain coupling is a common effect in such systems.

At the cost of adding more elements in a fiber laser sensor system, an alternative is to multiplex the fiber laser sensor in a parallel configuration. This system, in essence, incorporates several single fiber lasers, one for each fiber Bragg grating.

4. Simultaneous measurements of strain and temperature

Although Bragg gratings are well suited for measuring strain and temperature in a structure, one of the drawbacks is the actual separation of the temperature from the strain component. This complicates the Bragg grating application as a strain or a temperature gauge. On a single measurement of the Bragg wavelength shift, it is impossible to differentiate between the effects of changes in strain and temperature. Various schemes for discriminating between these effects have been developed. These include the use of a second grating element contained within a different material and placed in series with the first grating element[142] and the use of a pair of fiber grating surfaces mounted on an opposite surface of a bent mechanical structure.[143] However, these methods have limitations when it is required to interrogate the wavelength of a large number of fiber gratings. Techniques such as measuring two different wavelengths or two different optical modes[144,145] have been employed. In one other scheme, two superimposed fiber gratings having different Bragg wavelengths (850 and 1300 nm) have been used to simultaneously measure the strain and temperature (Fig. 61). The change in the Bragg wavelength of the fiber grating due to a combination of strain and temperature can be expressed as follows:

$$\Delta\lambda_B(\epsilon,\lambda)=\Psi_\epsilon\Delta\epsilon+\Psi_T\Delta T. \tag{6.4}$$

In the case where there are two Bragg gratings with different wavelengths (referred to as 1 and 2), then the following relation holds:

$$\begin{bmatrix}\Delta\lambda_{B_1}\\ \Delta\lambda_{B_2}\end{bmatrix}=\begin{bmatrix}\Psi_{\epsilon 1} & \Psi_{T1}\\ \Psi_{\epsilon 2} & \Psi_{T2}\end{bmatrix}\begin{bmatrix}\Delta\epsilon\\ \Delta T\end{bmatrix}. \tag{6.5}$$

The elements of the Ψ matrix can be determined experimentally by separately measuring the Bragg wavelength changes with strain and temperature. Once Ψ is known, changes in both strain and temperature can be determined using the inverse of Eq. (6.5). The measured values of Ψ obtained in Ref. 146 (for the fiber used in Ref. 146) were

$$\Psi_{\epsilon 1}=0.96\pm 6.5\times 10^{-3}\ \text{pm}/\mu\text{strain},$$

$$\Psi_{\epsilon 2}=0.59\pm 3.4\times 10^{-3}\ \text{pm}/\mu\text{strain},$$

$$\Psi_{T1}=8.72\times 7.7\times 10^{-2}\ \text{pm}/^\circ\text{C},$$

$$\Psi_{T2}=6.30\pm 3.7\times 10^{-2}\ \text{pm}/^\circ\text{C},$$

where $pm=1\times 10^{-12}$ m. If the inverse matrix is used, the strain and temperature may be obtained from the two wavelength shifts.

An alternative approach using a single Bragg grating has recently been demonstrated, combining the wavelength information from the first and second grating diffraction orders. This has been shown to provide similar temperature and strain separation to the above scheme, with the added advantage that only one grating is required.[147]

[1] K. O. Hill, Y. Fujii, D. C. Johnson, and B. S. Kawasaki, Appl. Phys. Lett. **32**, 647 (1978).
[2] B. S. Kawasaki, K. O. Hill, D. C. Johnson, and Y. Fujii, Opt. Lett. **3**, 66 (1978).
[3] G. Meltz, W. W. Morey, and W. H. Glenn, Opt. Lett. **14**, 823 (1989).
[4] K. O. Hill, B. Malo, F. Bilodeau, and D. C. Johnson, Annu. Rev. Mater. Sci. **23**, 125 (1993).
[5] R. J. Campbell and R. Kashyap, Int. J. Optoelectron. **9**, 33 (1994).
[6] R. Kashyap, Opt. Fiber Technol. **1**, 17 (1994).
[7] D. K. W. Lam and B. K. Garside, Appl. Opt. **20**, 440 (1981).
[8] J. Stone, J. Appl. Phys. **62**, 4371 (1987).
[9] P. St J. Russell, J.-L. Archambault, and L. Reekie, Phys. World **41**, (1993).
[10] J. M. Yeun, Appl. Opt. **21**, 136 (1982).
[11] D. L. Williams, S. T. Davey, R. Kashyap, J. R. Armitage, and B. J. Ainslie, Electron. Lett. **28**, 369 (1992).
[12] R. M. Atkins and V. Mizrahi, Electron. Lett. **28**, 1743 (1992).
[13] D. P. Hand and P. St. J. Russell, IOOC, Technical Digest, 21C3-21C4, Japan, 1989.
[14] K. O. Hill, B. Malo, F. Bilodeau, D. C. Johnson, T. F. Morse, A. Kilian, L. Reinhart, and O. Kyunghwan, Proceedings of the Conference on Optical Fiber Communications, OFC'91, 14, PD3-1, 1991.
[15] M. M. Broer, C. L. Cone, and J. R. Simpson, Opt. Lett. **16**, 1391 (1991).
[16] F. Bilodeau, D. C. Johnson, B. Malo, K. A. Vineberg, and K. O. Hill, Opt. Lett. **15**, 1138 (1990).
[17] D. L. Williams, B. J. Ainslie, J. R. Armitage, R. Kashyap, and R. J. Campbell, Electron. Lett. **29**, 1191 (1993).
[18] P. Niay, P. Bernage, T. Taunay, W. X. Xie, S. Boj, E. Delevaque, H. Poignant, and M. Monerie, Proceedings of the Conference on Lasers and Electro-Optics, CLEO'94, 21 Postdeadline Paper CPD9, 1994.
[19] P. J. Kaiser, J. Opt. Soc. Am. **64**, 475 (1974).
[20] E. J. Friebele, C. G. Askin, M. E. Gingerich, and K. J. Long, Nucl. Instrum. Methods Phys. Res. B **1**, 355 (1984).
[21] H. Kawazoe, Y. Watanabe, K. Shibuya, and K. Muta, Mater. Res. Soc. Symp. Proc. **61**, 350 (1986).
[22] P. St. J. Russell, L. J. Poyntz-Wright, and D. P. Hand, Proc. SPIE **1373**, 126 (1990).
[23] D. L. Griscom and E. J. Friebele, Phys. Rev. B **24**, 4896 (1981).
[24] R. M. Atkins, V. Mizrahi, and T. Erdogan, Electron. Lett. **29**, 385 (1993).
[25] E. J. Friebele and D. L. Griscom, Mater. Res. Soc. Symp. Proc. **61**, 319 (1986).
[26] T. E. Tsai and D. L. Griscom, Proc. SPIE **1516**, 14 (1991).
[27] P. St. J. Russel, D. P. M. Hand, Y. T. Chow, and L. J. Poyntz-Wright, Proc. SPIE **1516**, 47 (1991).
[28] M. G. Sceates, G. R. Atkins, and S. B. Poole, Annu. Rev. Mater. Sci. **23**, 381 (1993).
[29] P. J. Lemaire, R. M. Atkins, V. Mizrahi, and W. A. Reed, Electron. Lett. **29**, 1191 (1993).
[30] R. M. Atkins, P. J. Lemaire, T. Erdogan, and V. Mizrahi, Electron. Lett. **29**, 1234 (1993).

[31] K. Awazu, H. Kawazoe, and M. Yamane, J. Appl. Phys. **68**, 2713 (1990).
[32] K. Noguchi, N. Shibata, N. Uesugi, and Y. Negishi, J. Lightwave Technol. **LT-3**, 236 (1985).
[33] V. Mizrahi, P. J. Lemaire, T. E. Erdogan, W. A. Reed, D. J. DiGiovanni, and R. M. Atkins, Appl. Phys. Lett. **63**, 1727 (1993).
[34] F. Bilodeau, B. Malo, J. Albert, D. C. Johnson, and K. O. Hill, Opt. Lett. **18**, 953 (1993).
[35] D. L. Williams, B. J. Ainslie, R. Armitage, R. Kashyap, and R. Campbell, Electron. Lett. **29**, 45 (1993).
[36] I. Camlibel, D. A. Pinnow, and F. W. Dabby, Appl. Phys. Lett. **26**, 185 (1975).
[37] D. L. Williams, B. J. Ainslie, R. Kashyap, G. D. Maxwell, J. R. Armitage, R. J. Campbell, and R. Wyatt, Proc. SPIE **2044**, 55 (1993).
[38] J. Albert, B. Malo, F. Bilodeau, D. C. Johnson, K. O. Hill, Y. Hibino, and M. Kawachi, Opt. Lett. **19**, 387 (1994).
[39] P. E. Dyer, R. J. Farley, R. Giedl, K. C. Byron, and D. Reid, Electron. Lett. **30**, 860 (1994).
[40] D. P. Hand and P. St J. Russell, Opt. Lett. **15**, 102 (1990).
[41] I. Fertein, S. Legoubin, M. Douay, S. Canon, P. Bernage, and P. Niay, Electron. Lett. **27**, 1838 (1991).
[42] J. P. Bernardin and N. M. Lawandy, Opt. Commun. **79**, 194 (1990).
[43] C. Fiori and R. A. B. Devine, Mater. Res. Soc. Symp. Proc. **61**, 187 (1986).
[44] M. G. Sceats and S. B. Poole, Aust. Conf. Opt. Fiber Technol. 302 (1991).
[45] R. Kashyap, J. R. Armitage, R. Wyatt, S. T. Davey, and D. L. Williams, Electron. Lett. **26**, 730 (1990).
[46] B. J. Eggleton, P. A. Krug, and L. Poladian, Opt. Lett. **19**, 877 (1994).
[47] H. G. Limberger, P. Y. Fonjallaz, P. Lambelet, Salathe, Ch. Zimmer, and H. H. Gilgen, Proc. SPIE **2044**, 272 (1993).
[48] A. Othonos and X. Lee, Rev. Sci. Instrum. **66**, 3112 (1995).
[49] J. Cannon and S. Lee, Laser Focus World **2**, 50 (1994).
[50] K. O. Hill, B. Malo, F. Bilodeau, D. C. Johnson, and J. Albert, Appl. Phys. Lett. **62**, 1035 (1993).
[51] D. Z. Anderson, V. Mizrahi, T. Erdogan, and A. E. White, Proceedings of the Conference on Optical Fiber Communication, OFC'93, Technical Digest, p. 68, Postdeadline Paper PD16 (1993).
[52] D. Z. Anderson, V. Mizrahi, T. Erdogan, and A. E. White, Electron. Lett. **29**, 566 (1993).
[53] J. Albert, S. Theriault, F. Bilodeau, D. C. Johnson, K. O. Hill, P. Sixt, and M. J. Rooks, IEEE Photonics Technol. Lett. **8**, 1334 (1996).
[54] A. Othonos and X. Lee, IEEE Photonics Technol. Lett. **7**, 1183 (1995).
[55] P. E. Dyer, R. J. Farley, and R. Giedl, Opt. Commun. **115**, 327 (1995).
[56] R. Kashyap, J. R. Armitage, R. J. Campbell, D. L. Williams, G. D. Maxwell, B. J. Ainslie, and C. A. Millar, BT Technol. J. **11**, (1993).
[57] B. Malo, K. O. Hill, F. Bilodeau, D. C. Johnson, and J. Albert, Electron. Lett. **29**, 1668 (1993).
[58] K. O. Hill, B. Malo, K. A. Vineberg, F. Bilodeau, D. C. Johnson, and I. Skinner, Electron. Lett. **26**, 1270 (1990).
[59] K. O. Hill, F. Bilodeau, B. Malo, and D. C. Johnson, Electron. Lett. **27**, 1548 (1991).
[60] S. Mihailov and M. Gower, Electron. Lett. **30**, 707 (1994).
[61] W. W. Morey, G. Meltz, and W. H. Glenn, Proc. SPIE **1582**, 36 (1992).
[62] V. Mizrahi and J. E. Sipe, J. Lightwave Technol. **11**, 1513 (1993).
[63] E. Delevaque, S. Boj, J. F. Bayon, H. Poignat, J. Le Mellot, and M. Monerie, Opt. Fiber Commun. Conf. Paper PD5 (1995).
[64] T. Komukai and M. Nakazawa, Jpn. J. Appl. Phys., Part 2 **34**, L1286 (1995).
[65] L. Dong, L. Reekie, J. L. Cruz, J. E. Caplen, J. P. de Sandro, and D. N. Payne, IEEE Photonics Technol. Lett. **9**, 64 (1997).
[66] W. W. Morey, J. R. Dunphy, and G. Meltz, Proc. SPIE **1586**, (1991).
[67] G. A. Ball, W. W. Morey, and W. H. Glenn, IEEE Photonics Technol. Lett. **3**, 613 (1991).
[68] F. X. D'Amato and J. R. Dunphy, IEEE LEOS Conference Proceedings, Paper DLTA 7.3, Boston (1992).
[69] G. A. Ball and W. W. Morey, IEEE Photonics Technol. Lett. **3**, 1077 (1991).
[70] G. A. Ball and W. W. Morey, Opt. Lett. **17**, 420 (1992).
[71] A. Othonos, A. T. Alavie, S. Melle, S. E. Karr, and R. M. Measures, Opt. Eng. (Bellingham) **32**, 2841 (1993).
[72] A. D. Kersey and W. W. Morey, Electron. Lett. **29**, 112 (1993).
[73] A. T. Alavie, S. E. Karr, A. Othonos, and R. M. Measures, IEEE Photonics Technol. Lett. **5**, 1112 (1993).
[74] G. Meltz and W. W. Morey, OFC'91, TuM2 (1991).
[75] R. Kashyap, R. Wyatt, and P. F. Mckee, Electron. Lett. **29**, 1025 (1993).
[76] K. C. Byron, K. Sugden, T. Bircheno, and I. Bennion, Electron. Lett. **29**, 1659 (1993).
[77] K. Sugden, I. Bennion, A. Molony, and N. J. Copner, Electron. Lett. **30**, 440 (1994).
[78] J. Martin, J. Lauzon, S. Thibault, and F. Quellette, Proceedings of the Conference on Optical Fiber Communications, OFC'94, Postdeadline Paper PD29-1 (1994).
[79] K. O. Hill, F. Bilodeau, B. Malo, T. Kitagawa, S. Theriault, D. C. Johnson, and J. Albert, Proceedings of the Conference on Optical Fiber Communications, OFC'94, Technical Digest, Postdeadline Paper PD2-1 (1994).
[80] R. Kashyap, P. F. McKee, R. J. Campbell, and D. L. Williams, Electron. Lett. **30**, 996 (1994).
[81] M. C. Farries, C. M. Ragdale, and D. C. J. Reid, Conference on Optical Amplifiers and their Applications, Snowmass, pp. 144 (1991).
[82] C. R. Giles, J. Stone, L. W. Stulz, K. Walker, and C. A. Burrus, Conference on Optical Amplifiers and their Applications, Snowmass, pp. 148 (1991).
[83] M. C. Farries, C. M. Ragdale, and D. C. J. Reid, Electron. Lett. **28**, 487 (1992).
[84] J.-L. Archambault, L. Reekie, and P. St J. Russell, Electron. Lett. **29**, 453 (1993).
[85] G. Meltz and W. W. Morey, Proc. SPIE **1516**, 185 (1991).
[86] L. Dong, J.-L. Archambault, L. Reekie, P. St J. Russell, and D. N. Payne, Electron. Lett. **29**, 1577 (1993).
[87] C. G. Askins, M. A. Putnam, G. M. Williams, and E. J. Friebele, Opt. Lett. **19**, 147 (1994).
[88] A. Othonos, X. Lee, and R. M. Measures, Electron. Lett. **30**, 1972 (1994).
[89] B. J. Eggleton, P. A. Krug, L. Poladian, and F. Quellette, Electron. Lett. **30**, 1620 (1994).
[90] W. W. Morey, G. A. Ball, and G. Meltz, Opt. Photonics News **5**, 8 (1994).
[91] G. P. Agrawal and A. H. Bobeck, IEEE J. Quantum Electron. **24**, 2407 (1988).
[92] G. P. Agrawal and N. K. Dutta, *Semiconductor Lasers* (Van Nostrand Reinhold, New York, 1993), Chap. 7.
[93] H. A. Haus and C. V. Shank, IEEE J. Quantum Electron. **QE-12**, 352 (1976).
[94] R. C. Alferness, C. H. Joyner, M. D. Divino, M. J. R. Martyak, and L. L. Buhl, Appl. Phys. Lett. **49**, 125 (1986).
[95] K. Utaka, S. Akiba, K. Skai, and Y. Matsushima, IEEE J. Quantum Electron. **QE-22**, 1042 (1986).
[96] R. Kashyap, P. F. McKee, and D. Armes, Electron. Lett. **30**, 1977 (1994).
[97] J. Canning and M. G. Sceats, Electron. Lett. **30**, 1344 (1994).
[98] D. Uttamchandani and A. Othonos, Opt. Commun. **127**, 200 (1996).
[99] A. Yariv and M. Nakamura, IEEE J. Quantum Electron. **4**, 233 (1977).
[100] H. A. Haus, in *Waves and Fields in Optoelectronics*, edited by N. Holonyak (Prentice-Hall, Englewood Cliffs, New Jersey, 1984), Chap. 3, p. 78.
[101] M. Yamada and K. Sakuda, Appl. Opt. **26**, 3474 (1987).
[102] K. O. Hill, S. Theriault, B. Malo, f. Bilodeau, T. Kitigawa, D. C. Johnson, J. Albert, K. Takiguchi, T. Kataoka, and K. Hagimoto, Electron. Lett. **30**, 1755 (1994).
[103] V. Mizrahi and J. E. Sipe, J. Lightwave Technol. **LT-11**, 1513 (1993).
[104] J. Albert, K. O. Hill, B. Malo, S. Theriault, F. Bilodeau, D. C. Johnson, and L. E. Erickson, Electron. Lett. **31**, 222 (1995).
[105] B. Malo, S. Theriault, D. C. Johnson, f. Bilodeau, J. Albert, and K. O. Hill, Electron. Lett. **31**, 223 (1995).
[106] R. Kashyap, A. Swanton, and D. J. Armes, Electron. Lett. **32**, 1226 (1996).
[107] D. M. Bird, J. R. Armitage, R. Kashyap, R. M. A. Fatah, and K. H. Cameron, Electron. Lett. **27**, 1115 (1991).
[108] P. A. Morton, V. Mizrahi, P. J. Lemaire, T. Tanbun-Ek, R. A. Logan, H. M. Presby, T. Erdogan, S. L. Woodward, M. R. Phillips, A. M. Sergent, and K. W. Wecht, Proceedings of the Conference on Optical Fiber Communications, OFC'94, Paper WG4, 1994.
[109] P. A. Morton, V. Mizrahi, P. A. Andrekson, T. Tanbun-Ek, R. A. Logan, P. J. Lemaire, D. L. Coblentz, A. M. Sergent, K. W. Wecht, and P. F. Sciortino, Jr., IEEE Photonics Technol. Lett. **5**, 28 (1993).
[110] L. Reekie, R. J. Mears, S. B. Poole, and D. N. Payne, J. Lightwave Technol. **LT4**, 956 (1986).
[111] G. A. Ball, W. W. Morey, and J. P. Waters, Electron. Lett. **26**, 1829 (1990).
[112] G. A. Ball and W. H. Glenn, J. Lightwave Technol. **10**, 1338 (1992).

[113] G. A. Ball, W. H. Glenn, W. W. Morey, and P. K. Cheo, IEEE Photonics Technol. Lett. **5**, 649 (1993).
[114] G. A. Ball, W. W. Morey, and P. K. Cheo, IEEE Photonics Technol. Lett. **5**, 267 (1993).
[115] G. A. Ball and W. W. Morey, Proceedings of the Conference on Optical Fiber Communications, OFC'92, 97 (1992).
[116] V. Mizrahi, D. DiGiovanni, R. M. Atkins, Y. Park, and J.-M. P. Delavaux, J. Lightwave Technol. **11**, 2021 (1993).
[117] A. Othonos, X. Lee, and D. P. Tsai, Opt. Eng. (Bellingham) **35**, 1088 (1996).
[118] J. L. Zyskind, V. Mizrahi, D. J. Digiovanni, and J. W. Sulhoff, Electron. Lett. **28**, 1385 (1992).
[119] J. L. Zyskind, J. W. Sulhoff, P. D. Magill, K. C. Reichmann, V. Mizrahi, and D. J. Digiovanni, Electron. Lett. **29**, 1105 (1993).
[120] F. Sanchez, P. L. Boudec, P. L. Francois, and G. Stephan, Phys. Rev. A **48**, 2220 (1993).
[121] G. A. Ball and W. W. Morey, Tech. Dig. Opt. Fiber Commun. **13**, 97 (1992).
[122] J. T. Kringlebotn, P. R. Morkel, L. Reekie, J.-L. Archambault, and D. N. Payne, Proceedings of the 19th European Conference on Optical Communications, Montreaux **2**, 65 (1993).
[123] J. T. Kringlebotn, J.-L. Archambault, L. Reekie, J. E. Townsend, F. F. Vienne, and D. N. Payne, Electron. Lett. **30**, 972 (1994).
[124] D. C. Hanna, L. M. Januncey, R. M. Percival, R. G. Smart, P. J. Suni, J. E. Townsend, and A. C. Tropper, Electron. Lett. **24**, 1222 (1988).
[125] D. C. Hanna, R. M. Percival, R. G. Smart, and A. C. Tropper, Opt. Commun. **75**, 283 (1990).
[126] D. C. Hanna, R. M. Percival, R. G. Smart, J. E. Townsend, and A. C. Tropper, Electron. Lett. **25**, 953 (1989).
[127] J. Y. Allain, M. Monerie, and H. Poignant, Electron. Lett. **27**, 1513 (1991).
[128] S. Boj, E. Delevaque, J. Y. Allain, J. F. Bayon, P. Niay, and P. Bernage, Electron. Lett. **30**, 1019 (1994).
[129] W. W. Morey, OFC'91, San Diego, California PDP 20,96 (1991).
[130] K. O. Hill, D. C. Johnson, F. Bilodeau, and S. Faucher, Electron. Lett. **23**, 465 (1987).
[131] F. Bilodeau, B. Malo, D. C. Johnson, J. Albert, and K. O. Hill, Proceedings of the European Conference on Optical Communications, ECOC'93, p. 29 ThC12.8 (1993).
[132] F. Bilodeau, B. Malo, D. C. Johnson, J. Albert, and K. O. Hill, IEEE Photonics Technol. Lett. **6**, 80 (1994).
[133] C. M. Ragdale, T. J. Reid, D. C. J. Reid, A. C. Carter, and P. J. Williams, Electron. Lett. **28**, 712 (1992).
[134] J. A. R. Williams, I. Bennion, K. Sugden, and N. J. Doran, Electron. Lett. **30**, 985 (1994).
[135] S. M. Melle, K. Liu, and R. M. Measures, IEEE Photonics Technol. Lett. **4**, 516 (1992).
[136] C. G. Askins, M. A. Putnam, G. M. Williams, and E. J. Friebele, Proc. SPIE **2071**, 12 (1993).
[137] J. R. Dunphy, G. Ball, F. D'Amato, P. Ferrato, S. Inserra, A. Vanucci, and M. Varasi, Proc. SPIE **2071**, 2 (1993).
[138] M. G. Xu, H. Gieger, J.-L. Archambault, L. Reekie, and J. P. Dakin, Proc. SPIE **2071**, 59 (1993).
[139] D. A. Jackson, A. B. Lobo Ribeiro, L. Reekie, and J. L. Archambault, Opt. Lett. **18**, 1192 (1993).
[140] A. D. Kersey, T. A. Berkoff, and W. W. Morey, Electron. Lett. **28**, 236 (1992).
[141] K. Kalli, G. P. Brady, D. J. Webb, D. A. Jackson, L. Zhang, and I. Bennion, Opt. Lett. **20**, 2544 (1995).
[142] W. W. Morey, G. Meltz, and J. M. Welss, Proc. OFS'8, Monterey, Postdeadline Paper PD-4.4 1992.
[143] M. G. Xu, J.-L. Archambault, L. Reekie, and J. P. Dakin, Int. J. Optoelectron.
[144] F. Farahi, D. J. Webb, J. D. C. Jones, and D. A. Jackson, J. Lightwave Technol. **LT-18**, 138 (1990).
[145] B. Culshaw and C. Michie, *Proceedings of the International Symposium on Advanced Material for Lightwave Structures*, ESTEC (Noordwijk, The Netherlands, 1992), pp. 393.
[146] M. G. Xu, J.-L. Archambault, L. Reekie, and J. P. Dakin, Electron. Lett. **30**, 1085 (1994).
[147] G. P. Brady, K. Kalli, D. J. Webb, L. Reekie, J. L. Archambault, and D. A. Jackson, IEE Proc.: Optoelectron. **144**, 156 (1997).